Parkinson's Disease-Linked Kir4.2 Mutation R28C Leads to Loss of Ion Channel Function

Xiaoyi Chen[1], Rocio K. Finol-Urdaneta[2], Mo Chen[1,3,4], Alex Skye[1], Bingmiao Gao[5], David J. Adams[2]*, George D. Mellick[1,6]*, Linlin Ma[1,6]*

[1]Griffith Institute for Drug Discovery, Griffith University, QLD 4111, Australia
[2]School of Medical, Indigenous and Health Sciences, Molecular Horizons Research Institute University of Wollongong, NSW 2522, Australia
[3]Clem Jones Centre for Neurobiology and Stem Cell Research, Griffith University, Nathan, 4111, QLD, Australia
[4]Menzies Health Institute Queensland, Griffith University, Southport, QLD, 4222, Australia
[5]Engineering Research Center of Tropical Medicine Innovation and Transformation, Ministry of Education, Hainan Key Laboratory for Research and Development of Tropical Herbs, School of Pharmacy, Hainan Medical University, Haikou 571199, China
[6]School of Environment and Science, Griffith University, QLD 4111, Australia

*****Correspondence:
Linlin.ma@griffith.edu.au; g.mellick@griffith.edu.au; djadams@uow.edu.au

Abstract

Parkinson's disease (PD) is a complex progressive neurodegenerative disorder involving multiple pathogenetic factors, including oxidative stress, mitochondria dysfunction, neuroinflammation, and ion imbalance. Emerging evidence underscores the significant role of potassium channels in multiple aspects of PD etiology. We recently identified a PD-linked genetic mutation in the *KCNJ15* gene (*KCNJ15*$^{p.R28C}$), encoding the inwardly rectifying potassium channel Kir4.2, within a four-generation family with familial PD. The role of the Kir4.2 channel, especially in neurodegenerative diseases, remains largely unexplored. This study aimed to elucidate the impact of the *KCNJ15*$^{p.R28C}$ (Kir4.2^{R28C}) mutation on the biophysical and biochemical properties of Kir4.2. Employing Kir4.2-overexpressing HEK293T cells as our model, we investigated how the mutation affects the channel's biophysical properties, total protein expression, endoplasmic reticulum and lysosome processing, and plasma membrane trafficking. Patch clamp studies revealed that the Kir4.2^{R28C} mutation results in loss of channel function, exhibiting a strong dominant-negative effect. This can be partially attributed to the significantly diminished overall expression of the mutant channel protein compared to the wild-type (Kir4.2^{WT}). We observed that both Kir4.2^{WT} and Kir4.2^{R28C} proteins undergo glycosylation during the post-translational modification process, albeit with differing protein turnover efficiencies. Furthermore, the *KCNJ15*$^{p.R28C}$ mutation exhibits reduced stability compared to Kir4.2^{WT} and is more susceptible to protein recycling through the lysosomal degradation pathway. Additionally, Kir4.2^{R28C} displayed reduced

plasma membrane trafficking capacity compared to Kir4.2^{WT}. These findings suggest that the Kir4.2^{R28C} mutant possesses unique biomolecular and biophysical characteristics distinct from the Kir4.2^{WT} channel, which potentially elucidates its role in the pathogenesis of PD.

Introduction

Parkinson's disease (PD) is a complex and multifactorial neurodegenerative disorder characterized by the progressive degeneration of dopaminergic neurons in the substantia nigra pars compacta (SNpc) region of the midbrain, often accompanied by the presence of Lewy bodies throughout the central nervous system (Gibb and Lees 1988, Bloem, Okun and Klein 2021). Several factors have been implicated as potential risk factors for PD including ageing, exposure to environmental toxins, oxidative stress, dysfunctions in mitochondrial and lysosomal processes, and ion imbalance (Goldman 2014, Rodriguez *et al.* 2015). These factors can interact and create a cascade of cellular dysfunctions, increasing the vulnerability of dopaminergic (DA) neurons to neurodegeneration. DA neurons are known for their intrinsic pacemaker activity, a self-generated electrical rhythm crucial for their function, dependent on the coordinated activities of various ion channels including Na^+, Ca^{2+}, and K^+ channels (Cantrell and Catterall 2001, Pietrobon 2002, Kofuji and Newman 2004, Vaidya *et al.* 2024). Particularly, the pathogenetic significance of K^+ channels and K^+ homeostasis in PD is gaining momentum (Chen *et al.* 2023).

Inwardly rectifying potassium (Kir) channels are essential for maintaining K^+ balance, regulating the duration of action potentials, and influencing the resting membrane potential (Hibino *et al.* 2010, Baronas and Kurata 2014, Chen *et al.* 2023). The four sub-families, namely G protein-coupled (GIRK or Kir 3. x); ATP-sensitive (K_{ATP} or Kir6.x); classic (Kir2.x); and K^+ transport (Kir1.x; Kir4.x; Kir5.x, and Kir7.x). Kir channels, have distinctive structural and functional properties (Hibino *et al.* 2010). Several Kir channel family members have been demonstrated to play a critical role in PD pathogenesis (Chen *et al.* 2023). For example, the *Weaver* mouse model, characterized by a naturally occurring homozygous mutation, p.G156S, in the GIRK2 (Kir3.2) channel, exhibits a PD-like phenotype and has become an invaluable research tool extensively used in PD studies (Slesinger *et al.* 1996). This mutation converts GIRK2 from being highly selective for K^+ into a non-selective cation channel, resulting in increased excitotoxic stress in neurons, microglia-mediated neuroinflammation and subsequent neurodegeneration (Schmidt *et al.* 1982, Heginbotham, Abramson and MacKinnon 1992, Patil *et al.* 1995, Peng *et al.* 2006).

In a recent genetic linkage study employing whole exosome sequencing, we discovered a novel genetic variant, *KCNJ15*$^{p.R28C}$, that segregates strongly with PD in a big family with ten diagnosed PD patients across four generations. This variant is present in five PD cases and two unaffected individuals over the age of 80 within the family. Additionally, the same variant was found in other PD cases, including an isolated familial case in Italy with disease onset at 63 years and a sporadic PD patient in Australia with onset at 51 years (Bentley *et al.* 2021). This genetic evidence strongly suggests that *KCNJ15*-encoded protein, the inwardly rectifying potassium channel Kir4.2, may play a significant role in PD pathobiology, similar to other well-known genetic mutations such as *LRRK2*$^{p.G2019S}$, which contributes to disease with intermediate penetrance (Trinh, Guella and Farrer 2014, Hernandez, Reed and Singleton 2016). Interestingly, the *KCNJ15* gene was also found to be significantly associated with Alzheimer's disease (AD) in a large-scale genome-wide association study of AD, where *KCNJ15* was highly expressed in the immune system and involved in immune-related events (Zhou *et al.* 2018). Therefore, the Kir4.2 channel may represent a potential new molecular target for therapeutic intervention and biomarker development in neurodegenerative diseases.

The tetrameric Kir4.2 channel belongs to the K^+ transport channel subfamily of Kir channels, with each subunit consisting of 375 amino acids forming two transmembrane helices (Gosset *et al.* 1997, Shuck *et al.* 1997). The activation of the Kir4.2 channel is extracellular K^+- and intracellular pH-dependent with a single-channel conductance of ~25 pS and high open probability ($P_o \approx 0.7$-0.9) when the homotetrameric Kir4.2 is expressed in *Xenopus* oocytes (Pessia *et al.* 2001, Edvinsson, Shah and Palmer 2011). Although Kir4.2 is broadly expressed in various organs including the kidney, stomach, pancreas, and brain, its physiological functions remain largely elusive (Lourdel *et al.* 2002, He *et al.* 2011, Okamoto *et al.* 2012, Wang *et al.* 2022). It was only shown to inhibit insulin secretion in pancreatic β cells (Okamoto *et al.* 2010, Okamoto *et al.* 2012), regulate gastric acid secretion (He *et al.* 2011, Yuan *et al.* 2015), and may play an active role in epilepsy (Wang *et al.* 2022) and wound healing through regulating galvanotaxis (Nakajima *et al.* 2015, Nakajima and Zhao 2016). However, little is known about the biochemical properties of this channel protein and how they are affected by disease-associated mutations.

In this study, we aimed to understand how the genetic variant Kir4.2^{R28C} affects the channel protein's biophysical and biochemical functions. Kir4.2^{R28C} was found to be a loss-of-function mutation with a dominant-negative effect and our biochemical studies revealed a notable reduction in the overall expression of Kir4.2^{R28C} compared to Kir4.2^{WT} in transiently

transfected HEK293T cells. To determine the mechanism underlying this differential expression, posttranslational regulation, protein turnover in the cytoplasm, and the trafficking of the channel protein to the plasma membrane were studied in detail.

Results

In silico prediction of pathogenicity for the Kir4.2^{R28C} mutation

Kir4.2 channel functions either as a homo- or a hetero-tetramer in conjunction with Kir5.1, with each subunit comprising two transmembrane helices. The ion-conducting pore is predicated to be formed by amino acids 126-132, as suggested by similarity analysis (Pearson *et al.* 1999, Hibino *et al.* 2010). As shown in the AlphaFold-predicted 3D structure of the human Kir4.2 channel (Fig 1A), the amino acid change resulting from genetic variant p.R28C is located within the cytoplasmic N-terminal tail of the protein. Arg28 is poised to form hydrogen bonds with Pro27, and salt bridges with Glu278, Glu303, and Glu304 (Fig 1B). The mutation from the bulky, positively charged, and less hydrophobic Arg (Fig 1C) to smaller, more hydrophobic, neutral Cys (Fig 1D) could disrupt these critical interactions, potentially affecting the protein's tertiary and quaternary structures.

To assess the potential impact of the Kir4.2^{R28C} mutation, we conducted an *in silico* analysis using the bioinformatics platform HOPE (https://www3.cmbi.umcn.nl/hope/), which is a database for predicting the structural consequences of point mutations (Venselaar et al., 2010). The HOPE analysis assigned a MetaRNN score (ranging from 0.0 to 1.0) of 0.9605646 to Kir4.2^{R28C}, indicating that this mutation is highly likely to be pathogenic. This finding aligns with the assessment from another tool for scoring the deleteriousness of mutations, Combined Annotation Dependent Depletion (CADD, https://cadd.gs.washington.edu/), which assigned a Phred score of 16 to Kir4.2^{R28C}. This score positions Kir4.2^{R28C} among the top 2.5% of most deleterious substitutions, suggesting significant potential for pathogenicity (Rentzsch *et al.* 2019).

The Kir4.2^{R28C} mutation results in loss of ion channel function with a dominant-negative effect

The significance of a genetic mutation on an ion channel protein is largely determined by its impact on the ion-conducting functions and properties of the channel. To investigate the effects of the PD patient-derived Kir4.2^{R28C} mutation on channel biophysical features, we conducted

whole-cell patch clamp recordings in HEK293T cells. Cells were transiently transfected with wild-type ($Kir4.2^{WT}$) and mutant $Kir4.2^{R28C}$ cDNA, as well as a combination of both (WT+R28C). Inward rectifying K^+ currents were activated by a 400 ms voltage ramp from +150 mV to -150 mV from a holding potential of 0 mV in a symmetrical K^+ solution (see methods) (Figures 2).

Robust inward Ba^{2+}-sensitive currents were observed in cells transfected with $Kir4.2^{WT}$ channels recorded at -150 mV (CD^{WT} = -147.7 ± 23.1 pA/pF, n = 5), while a near-complete absence of Ba^{2+}-sensitive K^+ current was observed in cells transfected with $Kir4.2^{R28C}$ channels (CD^{R28C} = -8.4 ± 2.3 pA/pF, n = 7) (Figure 2A&B). Interestingly, cells transfected with equimolar amounts of $Kir4.2^{WT}$ and $Kir4.2^{R28C}$ constructs exhibited greatly reduced Ba^{2+}-sensitive inward currents ($CD^{WT+R28C}$ = -19.1 ± 3.2 pA/pF, n = 5) compared to homomeric $Kir4.2^{WT}$ channels (One-way ANOVA $P < 0.0001$) (Figure 2A&B), indicative of a dominant negative effect of the $Kir4.2^{R28C}$ mutant over $Kir4.2^{WT}$ currents.

The $Kir4.2^{R28C}$ mutation significantly reduces overall protein levels compared to $Kir4.2^{WT}$, with no impact on protein glycosylation.

The $Kir4.2^{R28C}$ mutation, located on the cytoplasmic N-tail of the channel protein (Fig. 1), is unlikely to directly affect the ion selectivity or conductivity through the channel pore. To understand the mechanism underlying the loss of function caused by such a mutation, we first compared the overall expression levels of $Kir4.2^{WT}$ and $Kir4.2^{R28C}$ transiently transfected in HEK293T cells using Western blot. Both $Kir4.2^{WT}$ and $Kir4.2^{R28C}$ exhibited two bands with apparent molecular weights of approximately 43 kDa and 45 kDa, respectively. However, the overall protein level of $Kir4.2^{R28C}$ was consistently lower than that of $Kir4.2^{WT}$ across biological replicates (Fig. 3A). Quantitative analysis revealed that the overall expression level of $Kir4.2^{R28C}$ was less than 50% of that observed for $Kir4.2^{WT}$ ($P < 0.0001$, N = 6, Fig. 3B). This finding is noteworthy given that both $Kir4.2^{WT}$ and $Kir4.2^{R28C}$ are expressed under the control of the same promoter within the same expression vector. The observed discrepancy in the overall protein levels suggests potential differences in post-translational modulations and/or protein turnover within the cells.

Kir4.2 channel has been predicted to undergo Asn-mediated N-linked glycosylation at positions 103 and 284 (Shuck *et al.* 1997, Pearson *et al.* 1999). Consequently, we proposed that the two distinct bands observed on the Western blot represent different glycosylation states of

the protein. N-linked Glycosylation involves the attachment of a glycan to the nitrogen atom in the side chain of asparagine within the consensus sequence Asn-X-Ser/Thr (where X can be any amino acid except proline). This glycan is initially processed in the ER, where certain glucose and mannose residues are removed – a crucial step for the proper folding and quality control of the glycoprotein. Misfolded glycoproteins are targeted for degradation, whereas correctly folded ones are transported to the Golgi apparatus for further processing. Here, the glycan is extensively modified, including the addition and removal of sugar residues, which significantly impact the glycoprotein's final function, localization, and stability (Fig 3C).

To assess whether Kir4.2^{R28C} exhibits the same glycosylation state and patterns as Kir4.2^{WT}, we treated the proteins with PNGase F and EndoH, respectively. PNGase F cleaves the bond between the innermost N-acetylglucosamine (GlcNAc) and the asparagine residue across all types of N-linked glycosylation. In contrast, Endo H targets the bond between the two GlcNAc residues of high-mannose and some hybrid types of N-linked oligosaccharides but does not act on complex glycans. Therefore, glycoproteins processed in the early Golgi stages are sensitive to Endo H, whereas those processed in the later stages are resistant to Endo H (Fig. 3C) (Tarentino, Gomez and Plummer 1985, Trimble and Tarentino 1991, Freeze and Kranz 2010). Treatment with PNGase F resulted in a single, lower molecular weight band for both Kir4.2^{WT} and Kir4.2^{R28C}, representing fully deglycosylated proteins (Fig. 3D). Although there was no statistical difference between the PNGase F treated Kir4.2^{WT} and Kir4.2^{R28C} proteins, Kir4.2^{WT} levels remained higher than Kir4.2^{R28C} (Fig. 3E). With Endo H treatment, Kir4.2^{R28C} exhibited a level approximately 50% of that observed for Kir4.2^{WT} ($P < 0.05$, N = 3, Fig. 3E). In addition, a significant proportion of proteins shifted from the higher (upper band) to the lower (bottom band) molecular weight band in both Kir4.2^{WT} and Kir4.2^{R28C}, altering the upper/bottom band ratos from >2 to <0.5 (Fig. 3D&3F). This finding indicates that most Kir4.2 channels are not fully glycosylated within the cell. Furthermore, the similarity in upper/bottom band ratios between Kir4.2^{WT} and Kir4.2^{R28C} suggests that Kir4.2^{R28C} exhibits comparable glycosylation states and patterns to Kir4.2^{WT}.

The stability and longevity of the Kir4.2^{R28C} mutant are reduced relative to Kir4.2^{WT}

Both PNGase F and EndoH are widely utilized to treat purified proteins, making them useful tools for analyzing the glycosylation state and patterns of protein products as static snapshots. However, they are not suitable for exploring the dynamics of protein glycosylation or its impact on protein stability over time within living cells. To investigate the effects of N-linked

glycosylation on Kir4.2^{WT} and Kir4.2^{R28C} within cells, we treated cells overexpressing Kir4.2^{WT} and Kir4.2^{R28C} with tunicamycin before extracting and analyzing the total proteins. Tunicamycin blocks N-linked glycosylation, potentially disrupting proper protein folding and function, thereby inducing cellular stress, the unfolded protein response (UPR), and the activation of stress pathways. Binding Immunoglobulin Protein (BiP), a marker of ER stress and UPR, served as a positive control (Fig. 4A), given its consistent and well-documented upregulation under such stress conditions across various cell types and experimental scenarios (Schroder and Kaufman 2005).

Interestingly, Kir4.2^{WT} and Kir4.2^{R28C} exhibited differing responses to tunicamycin treatment (Fig. 4). Kir4.2^{WT}'s overall expression and the ratio between mature and immature proteins were not significantly altered by tunicamycin (Fig. 4B&4C). In contrast, Kir4.2^{R28C} displayed a significant increase in overall protein levels following 6 h tunicamycin treatment ($P < 0.0001$, n = 4, Fig. 4B), along with a notable decrease in the proportion of mature proteins ($P < 0.05$, n = 4, Fig. 4C). Tunicamycin inhibits glycosylation by blocking the enzyme GlcNAc-1-P transferase, which catalyzes the first step in the synthesis of N-linked glycan precursors, therefore it primarily affects new glycosylation events when applied to cells post-transfection (Heifetz, Keenan and Elbein 1979, Wu *et al*. 2018). Given that both WT and mutant Kir4.2 proteins undergo N-glycosylation (Fig. 3C&3D), these findings suggest that the WT proteins might be more resilient to disruptions in glycosylation, potentially due to inherent stability and/or have a longer half-life compared to the mutant variants.

The Kir4.2^{R28C} mutant is more susceptible to autophagy-lysosomal degradation compared to Kir4.2^{WT}

Another crucial aspect influencing protein levels is protein degradation, an essential cellular function that manages protein turnover, ensures proteostasis, and eliminates damaged or misfolded proteins. Mammalian cells primarily utilize two pathways for protein degradation: the ubiquitin-proteasome system (UPS) and the autophagy-lysosomal pathway.

The UPS predominantly targets short-lived, misfolded, or damaged proteins for degradation. It has been implicated in the regulation of the biogenesis of Kir channels, such as the K_{ATP} channel (Yan *et al*. 2005, Steele, Eldstrom and Fedida 2007). Within this system, proteins destined for degradation are tagged with polyubiquitins and subsequently recognized and dismantled by the 26S proteasome, liberating ubiquitin for future use and decomposing the target protein into peptides (Fig. 5A). To explore the potential regulation of Kir4.2 by the UPS,

we employed the proteasome inhibitor MG132 to block UPS-mediated degradation (Fig. 5A) (Guo and Peng 2013, Kim and Kim 2020). MG132 was administered to HEK293T cells overexpressing Kir4.2^{WT} and Kir4.2^{R28C} 48 hours post-transfection for 8 hours (Fig. 5B). Despite MG132 treatment, the protein level of Kir4.2^{R28C} remained significantly lower than that of Kir4.2^{WT} ($P < 0.05$, N = 3, Fig. 5B&5C). Additionally, MG132 treatment did not significantly increase the protein levels of either Kir4.2^{WT} or Kir4.2^{R28C} (Fig. 5C), nor did it alter the ratio of mature to immature Kir channels (Fig. 5D). These results indicate that the UPS may not significantly influence Kir4.2 turnover within the cell.

The autophagy-lysosomal pathway is pivotal for degrading long-lived proteins, protein aggregates, and damaged organelles. It encapsulates the target materials in double-membraned autophagosomes, which subsequently fuse with lysosomes to form autolysosomes that degrade the encapsulated materials (Fig. 5A) (Dikic and Elazar 2018, Ballabio and Bonifacino 2020). The lysosomal degradation of membrane proteins, including Kir channels, has been well established (Jansen *et al.* 2008, Estadella *et al.* 2020, Hager *et al.* 2021) (Fig. 5A). Intriguingly, the Kir4.2 protein sequence harbours several LIR (LC3-Interacting Region) motifs, which bind to Atg8/LC3 protein family members to mediate autophagic processes, thereby tagging substrates for autophagy-lysosomal degradation (Geng and Klionsky 2008, Shpilka *et al.* 2011, Kumar *et al.* 2022).

To investigate the role of lysosomal degradation in the differential expression levels between Kir4.2^{WT} and Kir4.2^{R28C}, we administered bafilomycin A1 (Baf A1) to the cells. Baf A1 inhibits vacuolar-type H^+-ATPase (V-ATPase), effectively blocking lysosomal acidification and, consequently, autophagic flux, which is the process of autophagosome formation, fusion with lysosomes, and degradation of autophagic cargo (Yamamoto *et al.* 1998, Klionsky *et al.* 2008). LC3B (microtubule-associated protein 1A/1B-light chain 3B) is widely recognized as a key autophagy marker and plays a crucial role in the autophagosome formation process. The level of LC3B-II correlates with the number of autophagosomes in the cell, making it a reliable marker for monitoring autophagy flux. The inhibition of autophagic flux by bafilomycin A1 prevents the breakdown of autophagosomal contents, including LC3B-II, leading to its accumulation within the cell. Therefore, LC3B-II can be used as a positive control in this study (Lee and Lee 2016, Hwang and Kim 2023). As shown in Fig. 6A, with increased Baf A1 treatment, the level of LC3B-II was significantly elevated. Although not as pronounced as the increase in LC3B-II, a discernible trend showed that the overall levels of both Kir4.2^{WT} and Kir4.2^{R28C} rose with extended Baf A1 exposure (Fig. 6B). Notably, the baseline level of

Kir4.2^{R28C} was approximately 50% that of Kir4.2^{WT}, yet this difference vanished following a 6-hour Baf A1 treatment (Fig. 6B). This result suggests a crucial role for the autophagy-lysosomal pathway in the cellular recycling of Kir4.2 channels, where inhibiting this pathway appears to equalize the levels of Kir4.2^{R28C} to those of Kir4.2^{WT}. Furthermore, the ratios of mature to immature proteins for both Kir4.2^{WT} and Kir4.2^{R28C} demonstrated a decreasing trend with increased Baf A1 treatment (Fig. 6C), indicating a more targeted degradation of immature and potentially misfolded proteins via the autophagy-lysosomal pathway.

Kir4.2^{R28C} exhibits impaired membrane trafficking

Kir4.2 channels perform their physiological functions at the plasma membrane, making the study of their membrane trafficking, especially in mutant forms, essential. We utilized immunofluorescence to analyze the trafficking of Kir4.2^{WT} and Kir4.2^{R28C} in HEK293T cells as shown in Figures 7A&7B. The Na^+/K^+-ATPase, also known as the sodium-potassium pump, plays an essential role in maintaining homeostatic K^+ and Na^+ concentration gradients and is widely present in cell plasma membranes across various animal tissues. Due to its abundant expression at this location, it served as a plasma membrane marker in this and many other biological and biochemical studies (Zhang *et al*. 2015, Lobato-Alvarez *et al*. 2016, Schmid *et al*. 2022).

We observed that both Kir4.2^{WT} and Kir4.2^{R28C} channels are widely expressed within the cells, including at the plasma membrane. As expected, the overall expression levels of Kir4.2^{R28C} were significantly lower than those of Kir4.2^{WT} (Fig. 7A&7B), aligning with our Western blot findings (Fig 3). Analysis of cells expressing either Kir4.2^{WT} or Kir4.2^{R28C} (Fig 7C-7G) revealed a significantly higher colocalization of Kir4.2^{WT} with Na^+/K^+-ATPase at the plasma membrane than Kir4.2^{R28C} ($P < 0.01$, Fig 7H). However, considering the notably higher overall expression of Kir4.2^{WT} compared to Kir4.2^{R28C} (Figure 3), we sought to determine if the observed difference in membrane trafficking was solely attributable to differential expression levels. After normalizing the membrane trafficking data against the overall expression levels of Kir4.2, we found that the discrepancy between membrane-resident Kir4.2^{WT} and Kir4.2^{R28C} remained ($P < 0.05$, Fig 7I). These results require further verification using alternative methods. Nevertheless, current observations support the hypothesis that the mutation not only affects the stability and turnover of the Kir4.2 channel but also impairs the protein's plasma membrane trafficking capacity once it has been fully processed within the cell.

Discussion

PD is a complex and multifaceted neurodegenerative disorder. While the precise origins of PD remain elusive, genetic factors have been increasingly recognized as playing a crucial role in its pathogenesis (Gibb and Lees 1988, Poewe *et al.* 2017, Bloem, Okun and Klein 2021). The identification of specific genetic mutations linked to PD in both familial and sporadic cases has profoundly shaped our understanding of the disease mechanisms (Bonifati *et al.* 1995, Lill 2016). Notably, critical mutations on genes such as *SNCA* (α-synuclein) (Polymeropoulos *et al.* 1997), *PARK2* (Parkin) (Kitada *et al.* 1998), *PINK1* (PTEN-induced kinase 1) (Valente *et al.* 2001, Valente *et al.* 2004), *LRRK2* (Leucine-rich repeat kinase 2) (Funayama *et al.* 2002) , and *PARK7* (DJ-1) (Bonifati *et al.* 2003) have highlighted the significance of protein misfolding and aggregation in the disease pathogenesis, pinpointed mitochondrial dysfunction and oxidative stress as key pathological factors, unveiled new neuroinflammatory pathways that contribute to neuronal loss, and facilitated the development of animal and cellular models for the disease (Lill 2016, Poewe *et al.* 2017, Blauwendraat, Nalls and Singleton 2020). Among these PD-related genetic alterations, some are monogenic, directly causing the disease, whereas others are polygenic risk factors that, in combination with environmental influences and other genes, heighten the risk of developing the disease (Ross and Smith 2007, Lill 2016, Dunn, O'Connell and Kaczorowski 2019, Reed *et al.* 2019). These discoveries have paved the way for personalized medicine, allowing for treatments to be tailored to the genetic profile of individuals.

Recent studies are increasingly highlighting the involvement of potassium channels in the pathogenesis of PD (Chen *et al.* 2023). Beyond the well-characterized single mutation p.G156S in the GIRK2 (Kir3.2) channel, which causes parkinsonism in mice (Navarro *et al.* 1996, Liss, Neu and Roeper 1999), other potassium channels have also been identified as involved in PD (Chen *et al.* 2023). These include but are not limited to $K_V1.3$ (Tubert *et al.* 2016), $K_V2.1$ (Lebowitz *et al.* 2019), and Kir6.1 (Hu *et al.* 2019, Chen *et al.* 2021). In light of these insights, the identification of the novel mutation $Kir4.2^{R28C}$ in a PD family is noteworthy, potentially uncovering a new pathway involved in PD pathogenesis related to K^+ homeostasis and signaling.

Our electrophysiology studies reveal that the $Kir4.2^{R28C}$ homotetramers result in complete loss of channel function (Fig. 2). The profound functional impact of a mutation on the N-terminal cytoplasmic tail might seem counterintuitive. However, such mutations often disrupt the gating,

trafficking, or regulatory mechanisms of channels, a phenomenon observed across multiple channel types. For instance, cystic fibrosis is predominantly caused by a single mutation, ΔF508 (deletion of Phe508). This mutation leads to energetic instability and disrupts the folding and maturation of the channel protein, culminating in an almost complete loss of channel function (Lukacs *et al.* 1993, Lukacs *et al.* 1994, Jensen *et al.* 1995). In addition, genetic mutation R104W in the N-terminal of the $Na_V1.5$ channel abolishes the Na^+ currents and exerts a strong dominant-negative effect on wild-type channels, leading to Brugada syndrome. This condition is characterized by disruptions in cardiac electrical activity, leading to arrhythmias and sudden cardiac death (Clatot *et al.* 2012, Doisne *et al.* 2021).

More importantly, co-expressing $Kir4.2^{WT}$ and $Kir4.2^{R28C}$ at an equal molar ratio, which simulates the Kir4.2 heterotetramers found in *KCNJ15* family members with the heterozygous $Kir4.2^{R28C}$ mutation (Bentley *et al.* 2021), largely eliminates the function of WT channels (Fig. 2). This strong dominant-negative effect provides a compelling explanation for the association of the heterozygous $Kir4.2^{R28C}$ mutation with PD in this family and other sporadic PD cases.

Although our investigation of the *in vivo* implications of this loss-of-function mutation is still underway, this finding is particularly intriguing given that in neurons, Kir4.2 channels help set the resting membrane potential and regulate neuronal excitability. Abolished Kir4.2 function could lead to increased neuronal excitability, causing higher energy demands, and subsequently elevated mitochondrial activity and production of reactive oxygen species, which are known to contribute to neurodegeneration in PD (Orth and Schapira 2002, Drechsel and Patel 2008, Trist, Hare and Double 2019). The heightened excitability of neurons can also potentially lead to excessive glutamate release and activation of their receptors on neighboring neurons, resulting in excitotoxicity, a process where excessive stimulation of neurons leads to cell death (Caudle and Zhang 2009, Vaarmann *et al.* 2013, Wang *et al.* 2020). Furthermore, the basal ganglia, which are significantly affected in PD, rely on the delicate balance of excitatory and inhibitory signals to control movement (Aron and Poldrack 2006, Beste *et al.* 2010, Kumar *et al.* 2011). Increased excitability due to diminished Kir4.2 function can disrupt this balance, leading to chronic stress on neuronal networks which may contribute to their degeneration, exacerbating PD's progression.

Our *in vitro* studies also demonstrated that the $Kir4.2^{R28C}$ mutation exhibits a significantly reduced overall expression compared to $Kir4.2^{WT}$ (Fig 3A&3B). Given that the expression of both $Kir4.2^{WT}$ and $Kir4.2^{R28C}$ was driven by the same promoter under identical conditions using

model cell lines, it is more likely that this differential expression is caused by post-translational modifications, protein folding and turnover issues, which are crucial for the protein stability and function. Interestingly, similar to the ΔF508 mutation on the N-terminal tail of CFTR (Lukacs *et al.* 1993, Lukacs *et al.* 1994, Jensen *et al.* 1995), the mutant channel Kir4.2^{R28C} also exhibits decreased stability and longevity in cells compared to Kir4.2^{WT} (Fig 4). These findings suggest that the mutation may result in misfolded proteins, which are more likely to be recognized by the cell's quality control systems and targeted for degradation. Even if the protein folds initially, the mutation might cause conformational instability, making it more prone to unfolding or partial unfolding under physiological conditions. The accumulation of misfolded or unstable proteins in the ER can trigger the unfolded protein response, a cellular stress response for restoring normal function by halting protein translation, increasing the production of molecular chaperones, and enhancing the degradation of misfolded proteins (Friedlander *et al.* 2000, Flick and Kaiser 2012, Li, Li and Wu 2022).

Furthermore, misfolded proteins can aggregate, and these aggregates can impair mitochondrial function (Conway, Harper and Lansbury 1998, Tan, Wong and Lim 2009, Cox *et al.* 2018), leading to cellular stress and increased degradation via the autophagy-lysosomal pathway (Li *et al.* 2009, Ohta *et al.* 2009). Indeed, we found that Kir4.2 proteins are not primarily subjected to the ubiquitin-proteasome system-mediated degradation (Fig 5), but are more susceptible to the autophagy-lysosomal degradation pathway (Fig 6). Identifying the specific vulnerability of Kir4.2^{R28C} to degradation pathways opens the door for developing therapeutic interventions aimed at stabilizing the mutant channel or modulating the degradation pathways. For example, small molecules that enhance the stability of Kir4.2^{R28C} could potentially ameliorate the effects of the mutation.

Kir4.2 is identified as a glycosylated protein (Fig 3D-3F). The addition of carbohydrate groups can potentially protect the channel proteins from proteolytic degradation, thereby increasing their stability (Khanna *et al.* 2001, Russell, Oldham and Davis 2009, Lamothe *et al.* 2018). In addition, glycosylation serves as a crucial signal for cellular transport mechanisms, ensuring the accurate delivery of the channels to their designated location in the cell membrane (Gong *et al.* 2002, Fujita *et al.* 2006, Baycin-Hizal *et al.* 2014). Notably, despite the Kir4.2^{R28C} mutant displaying a glycosylation pattern similar to that of the Kir4.2^{WT} (Fig 2E & 2F), this mutation impairs the channel's ability to be trafficked to the plasma membrane (Fig 7). This impairment could stem from several factors, such as defective ER export or altered processing within the Golgi apparatus, both potentially caused by misfolding of the Kir4.2^{R28C} mutant, leading to ER

retention or disrupted sorting processes. Additionally, the mutation may influence the channel's internalization from the plasma membrane and subsequent recycling back to the surface. A disruption in the equilibrium between endocytosis and recycling could manifest as a reduced presence of the channel on the plasma membrane. Furthermore, the transportation of proteins to the plasma membrane is usually facilitated by a sophisticated array of adaptors, motors, and scaffold proteins (Tanemoto *et al.* 2002, Brasko *et al.* 2017, Zangerl-Plessl *et al.* 2019). While specific scaffold proteins associated with Kir4.2 remain unidentified, mutations might interfere with the interaction between Kir4.2 channels and these crucial proteins. Particularly, the Kir4.2^{R28C} mutant disrupts a PKB phosphorylation recognition site, a modification previously reported to affect the assembly and stability of the potassium channel/scaffold protein complex through phosphorylation (Tanemoto *et al.* 2002). These propositions warrant further exploration to elucidate the underlying mechanisms.

In summary, this study explored a novel genetic mutation in the Kir4.2 channel identified within a large PD family exhibiting multiple cases across four generations. Our findings reveal that this mutation leads to abolished channel function, diminished overall expression, and decreased stability of the Kir4.2 protein. Furthermore, there is an increased likelihood of lysosomal degradation and compromised plasma membrane trafficking of the mutant channel. These effects potentially exacerbate neuronal excitability, contributing to the pathogenesis of PD through mechanisms such as mitochondrial overactivity, elevated production of reactive oxygen species, and excitotoxicity. These findings not only deepen our understanding of PD but also pave the way for novel therapeutic approaches aimed at stabilizing affected potassium channels or modulating their degradation pathways. Ultimately, our study reinforces the value of genetic and molecular research in uncovering the intricacies of PD. By continuing to unravel the genetic contributions to PD, we move closer to personalized medicine approaches that can offer more effective, tailored treatments for individuals affected by this debilitating condition.

Materials and Methods

DNA constructs and mutagenesis

The cDNA of *KCNJ15*$^{p.R28C}$ was cloned from the primary olfactory neurosphere-derived cells (hONS) isolated from a mutation-carrying member in the family from which this new genetic variant was identified (Bentley *et al.* 2021). This cDNA was cloned into the pDONR201 vector (Addgene) and subsequently subcloned into the pcDNA3.1-ccdB-3xFLAG-V5 vector (Addgene) utilizing the Gateway cloning technique. To revert the *KCNJ15*$^{p.R28C}$ mutation to wildtype sequence, site-directed mutagenesis was performed using the pcDNA3.1-ccdB-3xFLAG-V5_ *KCNJ15*$^{p.R28C}$ construct DNA as a template. This process employed the KOD HiFi polymerase (Novagen), following the provided instructions. Specifically, the reaction mixture consisted of 50 ng template DNA, 0.2 mM dNTPs, 0.4 µM of each forward (5'-CAACAGACCCTGCGTCATGTCCAAGAGTGGGCAC-3') and reverse (5'-TTGGACATGACGCAGGGTCTGTTGGCCTTGAGCC-3') primer, 1 mM $MgCl_2$, 1U KOD HiFi PCR polymerase, and 1x KOD buffer. PCR conditions were set as follows: an initial denaturation at 95°C for 2 min, followed by 18 cycles of 95°C for 20 sec, 55°C for 10 sec, and 70°C for 130 sec, with a final extension at 70°C for 5 min. Mutagenic PCR products were then digested with 10 U DpnI (New England Biolabs) at 37°C for 30 min to eliminate template DNA. Successful mutagenesis was verified by full-length sequencing at the Griffith University DNA Sequencing Facility. Both *KCNJ15*$^{p.R28C}$ and *KCNJ15*^{WT} cDNAs were then sub-cloned into pIRES2-eGFP vector for patch-clamp studies.

Mammalian cell culture and transfection

HEK293T cells (ATCC) were cultured in Dulbecco's-Modified Eagle's Medium (DMEM) (Gibco), supplemented with 10% fetal bovine serum (FBS) (Merck), 2 mM GlutaMax (Life Technologies), and 100X MEM NEAA (Life Technologies) in a 37°C/5% CO_2 air-humidified incubator. For transfection, 10^5 cells were plated in 500 µl of culture media per well in a 24-well plate. After overnight incubation, the cells were transfected with 500 ng plasmid DNA using Lipofectamine 2000 (Invitrogen) with a DNA:Lipofectamine ratio of 1:6 according to the manufacturer's protocol. With tunicamycin (Sigma-Aldrich) or bafilomycin A1 (Sigma-Aldrich) treatment, transfected cells were exposed to the required concentrations for the specified duration before cell lysis.

Patch clamp electrophysiology

For patch-clamp studies, HEK293T cells were transiently transfected with Kir4.2^{WT}-pIRES2-eGFP and Kir4.2^{R28C}-pIRES2-eGFP constructs using Lipofectamine 2000 (Life Technologies) according to the manufacturer's instructions. At 18–24 h post-transfection, cells were mechanically dissociated, plated on glass coverslips and kept at 30°C, 5% CO_2 before recording.

Whole-cell currents of voltage-clamped cells were recorded by manual patch clamp electrophysiology according to standard protocols (Bony *et al*. 2022, Finol-Urdaneta *et al*. 2022) using a Multiclamp 700B amplifier connected to a computer and digitized with Digidata 1550 (Molecular Devices, San Jose, CA). GFP-positive transfected cells were identified using a Nikon Eclipse TS-100 fluorescence microscope. Pipettes were pulled from GC 150 F-15 borosilicate glass capillaries (Harvard Apparatus, Kent, UK) in five stages and fire-polished to 2-3 MΩ resistance when filled with intracellular solution containing (in mM): 140 K-Gluconate, 10 NaCl, 2 $MgCl_2$, 5 EGTA, and 10 HEPES, pH 7.2. Inward rectifier currents were recorded in a K^+-rich extracellular solution containing (in mM): 115 KCl, 30 NaCl, 5 glucose, 5 HEPES, 1 $CaCl_2$, 1 $MgSO_4$ (pH 7.4).

Data were acquired and analysed using pClamp 10 software (Molecular Devices). The series resistance was kept below 10 MΩ, and the cell capacitance was compensated by at least 70%. Membrane currents were sampled at 10 kHz and filtered at 1 kHz.

Inward rectifying K^+ currents were induced by 400 ms voltage ramps from +150 mV to -150 mV from a holding potential of 0 mV (0.1 Hz) at room temperature (21–23°C) in both control conditions and in the presence of 200 μM Ba^{2+}. Kir4.2 currents were calculated as the difference between the Ba^{2+}-sensitive component and the total inward current recorded at -150 mV. The resulting values were normalized by dividing by cell capacitance to obtain current density (pA/pF).

Western blot analysis

For immunoblot analysis, the cells in each well in a 25-well plate were harvested with 1000 µl ice-cold PBS and centrifuged at 300 g at 4°C for 10 min. The cell pellet was lyzed using 200 µl of lysis buffer (50 mM Tris, pH = 7.4; 150 mM NaCl; 1 mM EDTA; 0.25% Sodium deoxycholate; 0.1% SDS, plus 1% IGEPAL CA630), with the addition of 100X cOmplete™ Protease Inhibitor Cocktail (Roche) and PhosSTOP™ phosphatase inhibitor cocktail (Roche) before use. The cell lysate was homogenized by Branson S450A Sonifier cell disruptor (Output

30%, duty cycle 20, 10 s for 5 times), followed by centrifugation at 14,000 g at 4°C for 10 minutes. The total protein concentrations were quantified using the Pierce BCA Protein Assay kit (Thermo Fisher Scientific) following the manufacturer's protocol. For SDS-PAGE, protein samples (20 µg) were mixed with 5X SDS sample dye with 100 mM DTT, incubated at room temperature for 60 min, and stored at -20°C overnight. If required, protein samples were incubated with 500 U of PNGase F (New England Biolabs) or Endo H (New England Biolabs) at room temperature for 4 hours before being stored at -20°C overnight. The samples were centrifuged at 14,000 g for 30 seconds and loaded onto an SDS-PAGE gel (4% stacking gel and 12% resolving gel) in 1X SDS running buffer (25 mM Tris, 192 mM glycine, 0.1% SDS). PageRuler Plus Pre-Stained Protein ladder (Thermo Fisher Scientific) was used to estimate molecular weight. The gel was run at 150 V for one hour until the front of the dye had reached the bottom of the gel. Following SDS-PAGE separation, the proteins were transferred to a nitrocellulose membrane in a transfer buffer (25 mM Tris-base, 192 mM Glycine, 15% (v/v) Methanol) at 230 mA for 90 min. The membrane was blocked with 10 ml blocking buffer (5% BSA diluted in PBS-T (137 mM NaCl, 2.7 mM KCl, 10 mM Na_2HPO_4, 1.8 mM KH_2PO_4, 0.1% (w/v) Tween-20 detergent) or TBS-T (20 mM Tris-base, 150 mM NaCl, 0.1% (w/v) Tween-20 detergent) for 1 hour. The membrane was incubated with primary antibodies diluted in 3 ml PBS-T or TBS-T at room temperature and washed with PBS-T or TBS-T five times, for 5 minutes each time. The fluorophore-conjugated secondary antibodies were applied to the membrane for ~1 hour at room temperature. The membranes were imaged using the Odyssey® FC Imaging System (Li-COR). The primary antibodies included Rabbit mAb anti-V5-tag (D3H8Q) (Cell Signalling Technology, #13202S, 1:3000), Mouse mAb anti-FLAG M2 (Sigma-Aldrich, F1804, 1:20,000), Rabbit mAb anti-Bip (C50B12) (Cell Signalling Technology, #3177T, 1:3000), Mouse mAb anti-α-Tubulin (Sigma-Aldrich, T5168, 1:24,000). The secondary antibodies included IRDye® 680RD Donkey anti-Rabbit IgG (H + L) (LI-COR, 926-68073) and IRDye® 800CW Donkey anti-Mouse IgG (H + L) (LI-COR, 925-32212).

Immunofluorescence

For immunofluorescence experiments, transfected HEK293T cells were seeded on Poly-L-ornithine (Sigma-Aldrich, 0.0025%) pretreated coverslips at a density of 8000 cells/well (24 well) for 48-hour. The cells were fixed with 4% paraformaldehyde (PFA) on ice for 10 minutes, blocked and permeabilized with 80 µl blocking solution (10% Horse serum, 0.1% Triton X-100, diluted in PBS) for 1 hour at room temperature. The primary antibodies (anti-V5-tag (D3H8Q) (Cell Signalling Technology, #13202S, 1:3000), Rabbit pAb anti-KCNJ15 (Abcam,

ab200397, 1:3000) were applied to coverslips and incubated at room temperature for 90 minutes. The coverslips were washed with PBS before being incubated with secondary antibodies (Alexa Fluor™ 488 Donkey anti-Rabbit IgG (H+L) 1:1000, Alexa Fluor™ 555 Donkey anti-Mouse IgG (H+L), 1:1000) at room temperature for 90 minutes, and further treated with Hoechst (1:3000) at room temperature for 15 minutes before being mounted with ProLong Diamond Antifade Mountant (Thermofisher). The cells were imaged with the Olympus FV3000RS spectral confocal microscope using Olympus Fluoview software (Evident Scientific, Tokyo, Japan). Fluorescence intensities were quantified using ImageJ software (NIH, MD) and Rstudio.

Data analysis

Western blots were analyzed and quantified using ImageJ. The raw data were corrected for background subtraction before quantitative analysis. Signals were then normalized to the total protein loaded to each lane (20 µg/lane), with equal loading being determined using the housekeeping protein α-tubulin.

Using the cell image analysis software CellProfiler (Broad Institute) (Stirling *et al.* 2021), several key steps were followed in analyzing immunofluorescence images. The process began with cell nucleus segmentation, where unnecessary image features from nuclear stains, such as nucleoli, were eliminated. This was crucial when using DNA-based stains to prevent the formation of voids in the images, which could significantly impact the accuracy of quantifying the number and area of cell nuclei. Next, after identifying the cell nuclei, which appear as complete ellipses, the cells' positions were determined using the nuclei's central coordinates, in a process known as cytoplasm segmentation. The cytoplasm size was then expanded from these central points based on the median cell size in the image. The third step involved cell membrane segmentation to accurately delineate the plasma membrane area. Despite using confocal microscopy for segmented scanning, signals from the cell membrane above and below the cell can show up as positive signals in the cytoplasmic region, complicating the accurate identification of the cell membrane position. After identifying the entire cell membrane's fluorescent signals, cytoplasmic regions were excluded to enhance the depiction of the cell membrane area. Finally, to quantify the expression of Kir4.2 channels on the plasma membrane, the total fluorescent signals from Kir4.2 within the clearly defined membrane area were normalized to the total membrane area.

Results for all experiments were generated from >3 independent experiments and presented as mean ± standard deviation. Data was normally distributed around the mean. Student's unpaired t-test or one-way ANOVA was used for statistical analysis. Data were considered statistically significant when $P < 0.05$ (*), $P < 0.01$ (**), $P < 0.001$ (***), and $P < 0.0001$ (****).

References

Aron, A. R. and R. A. Poldrack (2006). "Cortical and subcortical contributions to Stop signal response inhibition: role of the subthalamic nucleus." J Neurosci **26**(9): 2424-2433.

Ballabio, A. and J. S. Bonifacino (2020). "Lysosomes as dynamic regulators of cell and organismal homeostasis." Nat Rev Mol Cell Biol **21**(2): 101-118.

Baronas, V. A. and H. T. Kurata (2014). "Inward rectifiers and their regulation by endogenous polyamines." Front Physiol **5**: 325.

Baycin-Hizal, D., A. Gottschalk, E. Jacobson, S. Mai, D. Wolozny, H. Zhang, S. S. Krag and M. J. Betenbaugh (2014). "Physiologic and pathophysiologic consequences of altered sialylation and glycosylation on ion channel function." Biochem Biophys Res Commun **453**(2): 243-253.

Bentley, S. R., I. Guella, H. E. Sherman, H. M. Neuendorf, A. M. Sykes, J. Y. Fowdar, P. A. Silburn, S. A. Wood, M. J. Farrer and G. D. Mellick (2021). "Hunting for Familial Parkinson's Disease Mutations in the Post Genome Era." Genes (Basel) **12**(3).

Beste, C., R. Willemssen, C. Saft and M. Falkenstein (2010). "Response inhibition subprocesses and dopaminergic pathways: basal ganglia disease effects." Neuropsychologia **48**(2): 366-373.

Blauwendraat, C., M. A. Nalls and A. B. Singleton (2020). "The genetic architecture of Parkinson's disease." Lancet Neurol **19**(2): 170-178.

Bloem, B. R., M. S. Okun and C. Klein (2021). "Parkinson's disease." Lancet **397**(10291): 2284-2303.

Bonifati, V., E. Fabrizio, N. Vanacore, M. De Mari and G. Meco (1995). "Familial Parkinson's disease: a clinical genetic analysis." Can J Neurol Sci **22**(4): 272-279.

Bonifati, V., P. Rizzu, M. J. van Baren, O. Schaap, G. J. Breedveld, E. Krieger, M. C. Dekker, F. Squitieri, P. Ibanez, M. Joosse, J. W. van Dongen, N. Vanacore, J. C. van Swieten, A. Brice, G. Meco, C. M. van Duijn, B. A. Oostra and P. Heutink (2003). "Mutations in the *DJ-1* gene associated with autosomal recessive early-onset parkinsonism." Science **299**(5604): 256-259.

Bony, A. R., J. R. McArthur, R. K. Finol-Urdaneta and D. J. Adams (2022). "Analgesic α-conotoxins modulate native and recombinant GIRK1/2 channels via activation of $GABA_B$ receptors and reduce neuroexcitability." Br J Pharmacol **179**(1): 179-198.

Brasko, C., V. Hawkins, I. C. De La Rocha and A. M. Butt (2017). "Expression of Kir4.1 and Kir5.1 inwardly rectifying potassium channels in oligodendrocytes, the myelinating cells of the CNS." Brain Struct Funct **222**(1): 41-59.

Cantrell, A. R. and W. A. Catterall (2001). "Neuromodulation of Na^+ channels: an unexpected form of cellular plasticity." Nat Rev Neurosci **2**(6): 397-407.

Caudle, W. M. and J. Zhang (2009). "Glutamate, excitotoxicity, and programmed cell death in Parkinson disease." Exp Neurol **220**(2): 230-233.

Chen, M. M., Z. L. Hu, J. H. Ding, R. H. Du and G. Hu (2021). "Astrocytic Kir6.1 deletion aggravates neurodegeneration in the lipopolysaccharide-induced mouse model of Parkinson's disease via astrocyte-neuron cross talk through complement C3-C3R signaling." Brain Behav Immun **95**: 310-320.

Chen, X., Y. Feng, R. J. Quinn, D. L. Pountney, D. R. Richardson, G. D. Mellick and L. Ma (2023). "Potassium Channels in Parkinson's Disease: Potential Roles in Its Pathogenesis and Innovative Molecular Targets for Treatment." Pharmacol Rev **75**(4): 758-788.

Clatot, J., A. Ziyadeh-Isleem, S. Maugenre, I. Denjoy, H. Liu, G. Dilanian, S. N. Hatem, I. Deschenes, A. Coulombe, P. Guicheney and N. Neyroud (2012). "Dominant-negative effect of SCN5A N-terminal mutations through the interaction of $Na_V1.5$ alpha-subunits." Cardiovasc Res **96**(1): 53-63.

Conway, K. A., J. D. Harper and P. T. Lansbury (1998). "Accelerated *in vitro* fibril formation by a mutant α-synuclein linked to early-onset Parkinson disease." Nat Med **4**(11): 1318-1320.

Cox, D., D. R. Whiten, J. W. P. Brown, M. H. Horrocks, R. San Gil, C. M. Dobson, D. Klenerman, A. M. van Oijen and H. Ecroyd (2018). "The small heat shock protein Hsp27 binds α-synuclein fibrils, preventing elongation and cytotoxicity." J Biol Chem **293**(12): 4486-4497.

Dikic, I. and Z. Elazar (2018). "Mechanism and medical implications of mammalian autophagy." Nat Rev Mol Cell Biol **19**(6): 349-364.

Doisne, N., M. Grauso, N. Mougenot, M. Clergue, C. Souil, A. Coulombe, P. Guicheney and N. Neyroud (2021). "*In vivo* Dominant-Negative Effect of an *SCN5A* Brugada Syndrome Variant." Front Physiol **12**: 661413.

Drechsel, D. A. and M. Patel (2008). "Role of reactive oxygen species in the neurotoxicity of environmental agents implicated in Parkinson's disease." Free Radic Biol Med **44**(11): 1873-1886.

Dunn, A. R., K. M. S. O'Connell and C. C. Kaczorowski (2019). "Gene-by-environment interactions in Alzheimer's disease and Parkinson's disease." Neurosci Biobehav Rev **103**: 73-80.

Edvinsson, J. M., A. J. Shah and L. G. Palmer (2011). "Potassium-dependent activation of Kir4.2 K^+ channels." J Physiol **589**(Pt 24): 5949-5963.

Estadella, I., O. Pedros-Gamez, M. Colomer-Molera, M. Bosch, A. Sorkin and A. Felipe (2020). "Endocytosis: A Turnover Mechanism Controlling Ion Channel Function." Cells **9**(8).

Finol-Urdaneta, R. K., R. Ziegman, Z. Dekan, J. R. McArthur, S. Heitmann, K. Luna-Ramirez, H. S. Tae, A. Mueller, H. Starobova, Y. K. Chin, J. S. Wingerd, E. A. B. Undheim, B. Cristofori-Armstrong, A. P. Hill, V. Herzig, G. F. King, I. Vetter, L. D. Rash, D. J. Adams and P. F. Alewood (2022). "Multitarget nociceptor sensitization by a promiscuous peptide from the venom of the King Baboon spider." Proc Natl Acad Sci U S A **119**(5).

Flick, K. and P. Kaiser (2012). "Protein degradation and the stress response." Semin Cell Dev Biol **23**(5): 515-522.

Freeze, H. H. and C. Kranz (2010). "Endoglycosidase and glycoamidase release of N-linked glycans." Curr Protoc Mol Biol **Chapter 17**: Unit 17 13A.

Friedlander, R., E. Jarosch, J. Urban, C. Volkwein and T. Sommer (2000). "A regulatory link between ER-associated protein degradation and the unfolded-protein response." Nat Cell Biol **2**(7): 379-384.

Fujita, T., I. Utsunomiya, J. Ren, Y. Matsushita, M. Kawai, S. Sasaki, K. Hoshi, T. Miyatake and K. Taguchi (2006). "Glycosylation and cell surface expression of $K_V1.2$ potassium channel are regulated by determinants in the pore region." Neurochem Res **31**(5): 589-596.

Funayama, M., K. Hasegawa, H. Kowa, M. Saito, S. Tsuji and F. Obata (2002). "A new locus for Parkinson's disease (*PARK8*) maps to chromosome 12p11.2-q13.1." Ann Neurol **51**(3): 296-301.

Geng, J. and D. J. Klionsky (2008). "The Atg8 and Atg12 ubiquitin-like conjugation systems in macroautophagy. 'Protein modifications: beyond the usual suspects' review series." EMBO Rep **9**(9): 859-864.

Gibb, W. R. and A. J. Lees (1988). "The relevance of the Lewy body to the pathogenesis of idiopathic Parkinson's disease." J Neurol Neurosurg Psychiatry **51**(6): 745-752.

Goldman, S. M. (2014). "Environmental toxins and Parkinson's disease." Annu Rev Pharmacol Toxicol **54**: 141-164.

Gong, Q., C. L. Anderson, C. T. January and Z. Zhou (2002). "Role of glycosylation in cell surface expression and stability of HERG potassium channels." Am J Physiol Heart Circ Physiol **283**(1): H77-84.

Gosset, P., G. A. Ghezala, B. Korn, M. L. Yaspo, A. Poutska, H. Lehrach, P. M. Sinet and N. Creau (1997). "A new inward rectifier potassium channel gene (*KCNJ15*) localized on chromosome 21 in the Down syndrome chromosome region 1 (DCR1)." Genomics **44**(2): 237-241.

Guo, N. and Z. Peng (2013). "MG132, a proteasome inhibitor, induces apoptosis in tumor cells." Asia Pac J Clin Oncol **9**(1): 6-11.

Hager, N. A., C. K. McAtee, M. A. Lesko and A. F. O'Donnell (2021). "Inwardly Rectifying Potassium Channel Kir2.1 and its "Kir-ious" Regulation by Protein Trafficking and Roles in Development and Disease." Front Cell Dev Biol **9**: 796136.

He, W., W. Liu, C. S. Chew, S. S. Baker, R. D. Baker, J. G. Forte and L. Zhu (2011). "Acid secretion-associated translocation of *KCNJ15* in gastric parietal cells." Am J Physiol Gastrointest Liver Physiol **301**(4): G591-600.

Heginbotham, L., T. Abramson and R. MacKinnon (1992). "A functional connection between the pores of distantly related ion channels as revealed by mutant K^+ channels." Science **258**(5085): 1152-1155.

Heifetz, A., R. W. Keenan and A. D. Elbein (1979). "Mechanism of action of tunicamycin on the UDP-GlcNAc:dolichyl-phosphate Glc-NAc-1-phosphate transferase." Biochemistry **18**(11): 2186-2192.

Hernandez, D. G., X. Reed and A. B. Singleton (2016). "Genetics in Parkinson disease: Mendelian versus non-Mendelian inheritance." J Neurochem **139 Suppl 1**: 59-74.

Hibino, H., A. Inanobe, K. Furutani, S. Murakami, I. Findlay and Y. Kurachi (2010). "Inwardly rectifying potassium channels: their structure, function, and physiological roles." Physiol Rev **90**(1): 291-366.

Hu, Z. L., T. Sun, M. Lu, J. H. Ding, R. H. Du and G. Hu (2019). "Kir6.1/K_{ATP} channel on astrocytes protects against dopaminergic neurodegeneration in the MPTP mouse model of Parkinson's disease via promoting mitophagy." Brain Behav Immun **81**: 509-522.

Hwang, H. J. and Y. K. Kim (2023). "The role of LC3B in autophagy as an RNA-binding protein." Autophagy **19**(3): 1028-1030.

Jansen, J. A., T. P. de Boer, R. Wolswinkel, T. A. van Veen, M. A. Vos, H. V. van Rijen and M. A. van der Heyden (2008). "Lysosome mediated Kir2.1 breakdown directly influences inward rectifier current density." Biochem Biophys Res Commun **367**(3): 687-692.

Jensen, T. J., M. A. Loo, S. Pind, D. B. Williams, A. L. Goldberg and J. R. Riordan (1995). "Multiple proteolytic systems, including the proteasome, contribute to CFTR processing." Cell **83**(1): 129-135.

Khanna, R., M. P. Myers, M. Laine and D. M. Papazian (2001). "Glycosylation increases potassium channel stability and surface expression in mammalian cells." J Biol Chem **276**(36): 34028-34034.

Kim, Y. M. and H. J. Kim (2020). "Proteasome Inhibitor MG132 is Toxic and Inhibits the Proliferation of Rat Neural Stem Cells but Increases BDNF Expression to Protect Neurons." Biomolecules **10**(11).

Kitada, T., S. Asakawa, N. Hattori, H. Matsumine, Y. Yamamura, S. Minoshima, M. Yokochi, Y. Mizuno and N. Shimizu (1998). "Mutations in the *parkin* gene cause autosomal recessive juvenile parkinsonism." Nature **392**(6676): 605-608.

Klionsky, D. J., Z. Elazar, P. O. Seglen and D. C. Rubinsztein (2008). "Does bafilomycin A1 block the fusion of autophagosomes with lysosomes?" Autophagy **4**(7): 849-850.

Kofuji, P. and E. A. Newman (2004). "Potassium buffering in the central nervous system." Neuroscience **129**(4): 1045-1056.

Kumar, A., S. Cardanobile, S. Rotter and A. Aertsen (2011). "The role of inhibition in generating and controlling Parkinson's disease oscillations in the Basal Ganglia." Front Syst Neurosci **5**: 86.

Kumar, M., S. Michael, J. Alvarado-Valverde, B. Meszaros, H. Samano-Sanchez, A. Zeke, L. Dobson, T. Lazar, M. Ord, A. Nagpal, N. Farahi, M. Kaser, R. Kraleti, N. E. Davey, R. Pancsa, L. B. Chemes and T. J. Gibson (2022). "The Eukaryotic Linear Motif resource: 2022 release." Nucleic Acids Res **50**(D1): D497-D508.

Lamothe, S. M., M. Hulbert, J. Guo, W. Li, T. Yang and S. Zhang (2018). "Glycosylation stabilizes hERG channels on the plasma membrane by decreasing proteolytic susceptibility." FASEB J **32**(4): 1933-1943.

Lebowitz, J. J., J. A. Pino, P. M. Mackie, M. Lin, C. Hurst, K. Divita, A. T. Collins, D. N. Koutzoumis, G. E. Torres and H. Khoshbouei (2019). "Clustered K_V2.1 decreases dopamine transporter activity and internalization." J Biol Chem **294**(17): 6957-6971.

Lee, Y. K. and J. A. Lee (2016). "Role of the mammalian ATG8/LC3 family in autophagy: differential and compensatory roles in the spatiotemporal regulation of autophagy." BMB Rep **49**(8): 424-430.

Li, Y., L. Dunn, E. Greggio, B. Krumm, G. S. Jackson, M. R. Cookson, P. A. Lewis and J. Deng (2009). "The R1441C mutation alters the folding properties of the ROC domain of *LRRK2*." Biochim Biophys Acta **1792**(12): 1194-1197.

Li, Y., S. Li and H. Wu (2022). "Ubiquitination-Proteasome System (UPS) and Autophagy Two Main Protein Degradation Machineries in Response to Cell Stress." Cells **11**(5).

Lill, C. M. (2016). "Genetics of Parkinson's disease." Mol Cell Probes **30**(6): 386-396.

Liss, B., A. Neu and J. Roeper (1999). "The *weaver* mouse *gain-of-function* phenotype of dopaminergic midbrain neurons is determined by coactivation of *wv*Girk2 and K_{ATP} channels." J Neurosci **19**(20): 8839-8848.

Lobato-Alvarez, J. A., M. L. Roldan, T. D. Lopez-Murillo, R. Gonzalez-Ramirez, J. Bonilla-Delgado and L. Shoshani (2016). "The Apical Localization of Na^+, K^+-ATPase in Cultured Human Retinal Pigment Epithelial Cells Depends on Expression of the β_2 Subunit." Front Physiol **7**: 450.

Lourdel, S., M. Paulais, F. Cluzeaud, M. Bens, M. Tanemoto, Y. Kurachi, A. Vandewalle and J. Teulon (2002). "An inward rectifier K^+ channel at the basolateral membrane of the mouse distal convoluted tubule: similarities with Kir4-Kir5.1 heteromeric channels." J Physiol **538**(Pt 2): 391-404.

Lukacs, G. L., X. B. Chang, C. Bear, N. Kartner, A. Mohamed, J. R. Riordan and S. Grinstein (1993). "The ΔF508 mutation decreases the stability of cystic fibrosis transmembrane conductance regulator in the plasma membrane. Determination of functional half-lives on transfected cells." J Biol Chem **268**(29): 21592-21598.

Lukacs, G. L., A. Mohamed, N. Kartner, X. B. Chang, J. R. Riordan and S. Grinstein (1994). "Conformational maturation of CFTR but not its mutant counterpart (ΔF508) occurs in the endoplasmic reticulum and requires ATP." EMBO J **13**(24): 6076-6086.

Nakajima, K. and M. Zhao (2016). "Concerted action of *KCNJ15*/Kir4.2 and intracellular polyamines in sensing physiological electric fields for galvanotaxis." Channels (Austin) **10**(4): 264-266.

Nakajima, K. I., K. Zhu, Y. H. Sun, B. Hegyi, Q. Zeng, C. J. Murphy, J. V. Small, Y. Chen-Izu, Y. Izumiya, J. M. Penninger and M. Zhao (2015). "*KCNJ15*/Kir4.2 couples with polyamines to sense weak extracellular electric fields in galvanotaxis." Nat Commun **6**: 8532.

Navarro, B., M. E. Kennedy, B. Velimirovic, D. Bhat, A. S. Peterson and D. E. Clapham (1996). "Nonselective and G betagamma-insensitive weaver K^+ channels." Science **272**(5270): 1950-1953.

Ohta, E., Y. Katayama, F. Kawakami, M. Yamamoto, K. Tajima, T. Maekawa, N. Iida, S. Hattori and F. Obata (2009). "$I^{2020}T$ leucine-rich repeat kinase 2, the causative mutant molecule of familial Parkinson's disease, has a higher intracellular degradation rate than the wild-type molecule." Biochem Biophys Res Commun **390**(3): 710-715.

Okamoto, K., N. Iwasaki, K. Doi, E. Noiri, Y. Iwamoto, Y. Uchigata, T. Fujita and K. Tokunaga (2012). "Inhibition of glucose-stimulated insulin secretion by *KCNJ15*, a newly identified susceptibility gene for type 2 diabetes." Diabetes **61**(7): 1734-1741.

Okamoto, K., N. Iwasaki, C. Nishimura, K. Doi, E. Noiri, S. Nakamura, M. Takizawa, M. Ogata, R. Fujimaki, N. Grarup, C. Pisinger, K. Borch-Johnsen, T. Lauritzen, A. Sandbaek, T. Hansen, K. Yasuda, H. Osawa, K. Nanjo, T. Kadowaki, M. Kasuga, O. Pedersen, T. Fujita, N. Kamatani, Y. Iwamoto and K. Tokunaga (2010). "Identification of *KCNJ15* as a

susceptibility gene in Asian patients with type 2 diabetes mellitus." Am J Hum Genet **86**(1): 54-64.

Orth, M. and A. H. Schapira (2002). "Mitochondrial involvement in Parkinson's disease." Neurochem Int **40**(6): 533-541.

Patil, N., D. R. Cox, D. Bhat, M. Faham, R. M. Myers and A. S. Peterson (1995). "A potassium channel mutation in weaver mice implicates membrane excitability in granule cell differentiation." Nat Genet **11**(2): 126-129.

Pearson, W. L., M. Dourado, M. Schreiber, L. Salkoff and C. G. Nichols (1999). "Expression of a functional Kir4 family inward rectifier K^+ channel from a gene cloned from mouse liver." J Physiol **514 (Pt 3)**(Pt 3): 639-653.

Peng, J., L. Xie, F. F. Stevenson, S. Melov, D. A. Di Monte and J. K. Andersen (2006). "Nigrostriatal dopaminergic neurodegeneration in the weaver mouse is mediated via neuroinflammation and alleviated by minocycline administration." J Neurosci **26**(45): 11644-11651.

Pessia, M., P. Imbrici, M. C. D'Adamo, L. Salvatore and S. J. Tucker (2001). "Differential pH sensitivity of Kir4.1 and Kir4.2 potassium channels and their modulation by heteropolymerisation with Kir5.1." J Physiol **532**(Pt 2): 359-367.

Pietrobon, D. (2002). "Calcium channels and channelopathies of the central nervous system." Mol Neurobiol **25**(1): 31-50.

Poewe, W., K. Seppi, C. M. Tanner, G. M. Halliday, P. Brundin, J. Volkmann, A. E. Schrag and A. E. Lang (2017). "Parkinson disease." Nat Rev Dis Primers **3**: 17013.

Polymeropoulos, M. H., C. Lavedan, E. Leroy, S. E. Ide, A. Dehejia, A. Dutra, B. Pike, H. Root, J. Rubenstein, R. Boyer, E. S. Stenroos, S. Chandrasekharappa, A. Athanassiadou, T. Papapetropoulos, W. G. Johnson, A. M. Lazzarini, R. C. Duvoisin, G. Di Iorio, L. I. Golbe and R. L. Nussbaum (1997). "Mutation in the α-synuclein gene identified in families with Parkinson's disease." Science **276**(5321): 2045-2047.

Reed, X., S. Bandres-Ciga, C. Blauwendraat and M. R. Cookson (2019). "The role of monogenic genes in idiopathic Parkinson's disease." Neurobiol Dis **124**: 230-239.

Rentzsch, P., D. Witten, G. M. Cooper, J. Shendure and M. Kircher (2019). "CADD: predicting the deleteriousness of variants throughout the human genome." Nucleic Acids Res **47**(D1): D886-D894.

Rodriguez, M., C. Rodriguez-Sabate, I. Morales, A. Sanchez and M. Sabate (2015). "Parkinson's disease as a result of aging." Aging Cell **14**(3): 293-308.

Ross, C. A. and W. W. Smith (2007). "Gene-environment interactions in Parkinson's disease." Parkinsonism Relat Disord **13 Suppl 3**: S309-315.

Russell, D., N. J. Oldham and B. G. Davis (2009). "Site-selective chemical protein glycosylation protects from autolysis and proteolytic degradation." Carbohydr Res **344**(12): 1508-1514.

Schmid, V., A. Wurzel, C. H. Wetzel, K. Plossl, A. Bruckmann, P. Luckner, B. H. F. Weber and U. Friedrich (2022). "Retinoschisin and novel Na^+/K^+-ATPase interaction partners $K_V2.1$ and $K_V8.2$ define a growing protein complex at the inner segments of mammalian photoreceptors." Cell Mol Life Sci **79**(8): 448.

Schmidt, M. J., B. D. Sawyer, K. W. Perry, R. W. Fuller, M. M. Foreman and B. Ghetti (1982). "Dopamine deficiency in the *weaver* mutant mouse." J Neurosci **2**(3): 376-380.

Schroder, M. and R. J. Kaufman (2005). "The mammalian unfolded protein response." Annu Rev Biochem **74**: 739-789.

Shpilka, T., H. Weidberg, S. Pietrokovski and Z. Elazar (2011). "Atg8: an autophagy-related ubiquitin-like protein family." Genome Biol **12**(7): 226.

Shuck, M. E., T. M. Piser, J. H. Bock, J. L. Slightom, K. S. Lee and M. J. Bienkowski (1997). "Cloning and characterization of two K^+ inward rectifier (Kir) 1.1 potassium channel homologs from human kidney (Kir1.2 and Kir1.3)." J Biol Chem **272**(1): 586-593.

Slesinger, P. A., N. Patil, Y. J. Liao, Y. N. Jan, L. Y. Jan and D. R. Cox (1996). "Functional effects of the mouse weaver mutation on G protein-gated inwardly rectifying K^+ channels." Neuron **16**(2): 321-331.

Steele, D. F., J. Eldstrom and D. Fedida (2007). "Mechanisms of cardiac potassium channel trafficking." J Physiol **582**(Pt 1): 17-26.

Stirling, D. R., M. J. Swain-Bowden, A. M. Lucas, A. E. Carpenter, B. A. Cimini and A. Goodman (2021). "CellProfiler 4: improvements in speed, utility and usability." BMC Bioinformatics **22**(1): 433.

Tan, J. M., E. S. Wong and K. L. Lim (2009). "Protein misfolding and aggregation in Parkinson's disease." Antioxid Redox Signal **11**(9): 2119-2134.

Tanemoto, M., A. Fujita, K. Higashi and Y. Kurachi (2002). "PSD-95 mediates formation of a functional homomeric Kir5.1 channel in the brain." Neuron **34**(3): 387-397.

Tarentino, A. L., C. M. Gomez and T. H. Plummer, Jr. (1985). "Deglycosylation of asparagine-linked glycans by peptide: N-glycosidase F." Biochemistry **24**(17): 4665-4671.

Trimble, R. B. and A. L. Tarentino (1991). "Identification of distinct endoglycosidase (endo) activities in Flavobacterium meningosepticum: endo F1, endo F2, and endo F3. Endo F1 and endo H hydrolyze only high mannose and hybrid glycans." J Biol Chem **266**(3): 1646-1651.

Trinh, J., I. Guella and M. J. Farrer (2014). "Disease penetrance of late-onset parkinsonism: a meta-analysis." JAMA Neurol **71**(12): 1535-1539.

Trist, B. G., D. J. Hare and K. L. Double (2019). "Oxidative stress in the aging substantia nigra and the etiology of Parkinson's disease." Aging Cell **18**(6): e13031.

Tubert, C., I. R. E. Taravini, E. Flores-Barrera, G. M. Sanchez, M. A. Prost, M. E. Avale, K. Y. Tseng, L. Rela and M. G. Murer (2016). "Decrease of a Current Mediated by $K_V1.3$ Channels Causes Striatal Cholinergic Interneuron Hyperexcitability in Experimental Parkinsonism." Cell Rep **16**(10): 2749-2762.

Vaarmann, A., S. Kovac, K. M. Holmstrom, S. Gandhi and A. Y. Abramov (2013). "Dopamine protects neurons against glutamate-induced excitotoxicity." Cell Death Dis **4**(1): e455.

Vaidya, B., D. S. Padhy, H. C. Joshi, S. S. Sharma and J. N. Singh (2024). "Ion Channels and Metal Ions in Parkinson's Disease: Historical Perspective to the Current Scenario." Methods Mol Biol **2761**: 529-557.

Valente, E. M., P. M. Abou-Sleiman, V. Caputo, M. M. Muqit, K. Harvey, S. Gispert, Z. Ali, D. Del Turco, A. R. Bentivoglio, D. G. Healy, A. Albanese, R. Nussbaum, R. Gonzalez-Maldonado, T. Deller, S. Salvi, P. Cortelli, W. P. Gilks, D. S. Latchman, R. J. Harvey, B. Dallapiccola, G. Auburger and N. W. Wood (2004). "Hereditary early-onset Parkinson's disease caused by mutations in *PINK1*." Science **304**(5674): 1158-1160.

Valente, E. M., A. R. Bentivoglio, P. H. Dixon, A. Ferraris, T. Ialongo, M. Frontali, A. Albanese and N. W. Wood (2001). "Localization of a novel locus for autosomal recessive early-onset parkinsonism, *PARK6*, on human chromosome 1p35-p36." Am J Hum Genet **68**(4): 895-900.

Varadi, M., S. Anyango, M. Deshpande, S. Nair, C. Natassia, G. Yordanova, D. Yuan, O. Stroe, G. Wood, A. Laydon, A. Zidek, T. Green, K. Tunyasuvunakool, S. Petersen, J. Jumper, E. Clancy, R. Green, A. Vora, M. Lutfi, M. Figurnov, A. Cowie, N. Hobbs, P. Kohli, G. Kleywegt, E. Birney, D. Hassabis and S. Velankar (2022). "AlphaFold Protein Structure Database: massively expanding the structural coverage of protein-sequence space with high-accuracy models." Nucleic Acids Res **50**(D1): D439-D444.

Wang, J., F. Wang, D. Mai and S. Qu (2020). "Molecular Mechanisms of Glutamate Toxicity in Parkinson's Disease." Front Neurosci **14**: 585584.

Wang, S., Z. Li, X. Ding, Z. Zhao, M. Zhang, H. Xu, J. Lu and L. Dai (2022). "Integrative Analyses Identify *KCNJ15* as a Candidate Gene in Patients with Epilepsy." Neurol Ther **11**(4): 1767-1776.

Waterhouse, A., M. Bertoni, S. Bienert, G. Studer, G. Tauriello, R. Gumienny, F. T. Heer, T. A. P. de Beer, C. Rempfer, L. Bordoli, R. Lepore and T. Schwede (2018). "SWISS-MODEL: homology modelling of protein structures and complexes." Nucleic Acids Res **46**(W1): W296-W303.

Wu, J., S. Chen, H. Liu, Z. Zhang, Z. Ni, J. Chen, Z. Yang, Y. Nie and D. Fan (2018). "Tunicamycin specifically aggravates ER stress and overcomes chemoresistance in multidrug-resistant gastric cancer cells by inhibiting N-glycosylation." J Exp Clin Cancer Res **37**(1): 272.

Yamamoto, A., Y. Tagawa, T. Yoshimori, Y. Moriyama, R. Masaki and Y. Tashiro (1998). "Bafilomycin A1 prevents maturation of autophagic vacuoles by inhibiting fusion between autophagosomes and lysosomes in rat hepatoma cell line, H-4-II-E cells." Cell Struct Funct **23**(1): 33-42.

Yan, F. F., C. W. Lin, E. A. Cartier and S. L. Shyng (2005). "Role of ubiquitin-proteasome degradation pathway in biogenesis efficiency of β-cell ATP-sensitive potassium channels." Am J Physiol Cell Physiol **289**(5): C1351-1359.

Yuan, J., W. Liu, S. Karvar, S. S. Baker, W. He, R. D. Baker, G. Ji, J. Xie and L. Zhu (2015). "Potassium channel KCNJ15 is required for histamine-stimulated gastric acid secretion." Am J Physiol Cell Physiol **309**(4): C264-270.

Zangerl-Plessl, E. M., M. Qile, M. Bloothooft, A. Stary-Weinzinger and M. A. G. van der Heyden (2019). "Disease Associated Mutations in Kir Proteins Linked to Aberrant Inward Rectifier Channel Trafficking." Biomolecules **9**(11).

Zhang, B., Y. Yan, J. Jin, H. Lin, Z. Li, X. Zhang, J. Liu, C. Xi, A. Lieber, X. Fan and L. Ran (2015). "Two types of functionally distinct fiber containing structural protein complexes are produced during infection of adenovirus serotype 5." PLoS One **10**(2): e0117976.

Zhou, X., Y. Chen, K. Y. Mok, Q. Zhao, K. Chen, Y. Chen, J. Hardy, Y. Li, A. K. Y. Fu, Q. Guo, N. Y. Ip and I. Alzheimer's Disease Neuroimaging (2018). "Identification of genetic risk factors in the Chinese population implicates a role of immune system in Alzheimer's disease pathogenesis." Proc Natl Acad Sci U S A **115**(8): 1697-1706.

Acknowledgements

This work was supported by the Michael J Fox Foundation (MJFF-021285).

Author Contribution

X.C performed the molecular biology and cell biology experiments, analyzed data, and drafted the original manuscript; R.F.K conducted the patch clamp studies and wrote the corresponding methods and results; M. C designed and performed the immunofluorescence data analysis; A.S and B.G helped with the research design and resources; D.J.A, G.D.M, and L.M designed and supervised the research. All the authors contributed to the manuscript editing.

Declaration Of Interest

The authors declare no competing interests.

Figure Legends

Figure 1 The 3D structural model of the Kir4.2 channel by the AlphaFold. (**A**) Predicted 3D structure of Kir4.2 channel protein (KCNJ15, accessible at https://alphafold.ebi.ac.uk/)(Varadi *et al.* 2022), illustrating a single subunit of the tetrameric channel. Arginine at position 28 (R28) is marked with a red circle. AlphaFold produces a per-residue confidence score (pLDDT) between 0 and 100. Blue pLDDT >90; Cyan 90>pLDDT>70; Yellow 70>pLDDT>50; Red pLDDT<50. The model's average confidence score is 0.85. (**B**) A zoomed-in view of the highlighted R28 area and adjacent residues, with R28 emphasized in pink. Dashed lines indicate potential hydrogen bonding. (**C-D**) Detailed visualization of the R28C mutation in Kir4.2 protein (accessible at SWISS-MODEL *https://swissmodel.expasy.org/interactive*)(Waterhouse *et al.* 2018, Varadi *et al.* 2022) with structures of the wild-type Arginine (C) and the mutant residue Cysteine (D) highlighted. In the highlighted amino acid, blue represents the amino group, yellow represents the *thiol* group, and red represents the carbonyl group, respectively.

Figure 2 The Kir4.2^{R28C} mutation significantly reduces the current density of recombinant Kir4.2 channels. (A) Representative whole-cell current traces obtained from HEK293T cells transiently transfected with Kir4.2^{WT}, Kir4.2^{R28C}, and Kir4.2$^{WT+R28C}$. The stimulus (inset) consisted of a 400 ms ramp from 150 mV to -150 mV, from a holding potential (Vh) of 0 mV. The Ba^{2+}-sensitive current components of cells over-expressing Kir4.2^{WT}, Kir4.2^{R28C}, and Kir4.2$^{WT+R28C}$ are shaded in blue, orange, and purple, respectively. **(B)** Summary data presented as a violin plot of current density (pA/pF measured at -150 mV) for Ba^{2+}-sensitive currents mediated by Kir4.2^{WT} (n = 5), Kir4.2^{R28C} (n = 7), and co-expressed Kir4.2$^{WT+R28C}$ (n = 5). Statistical analysis was conducted using One-way ANOVA (**** P < 0.0001).

Figure 3 Comparative analysis of Kir4.2^{WT} and Kir4.2^{R28C} in overall protein expression and glycosylation. (A) Western blot analysis of the protein expression levels of Kir4.2^{WT} and

Kir4.2^{R28C} in transiently transfected HEK293T cells. NT, Non-transfected; WT, Kir4.2^{WT}; MT, Kir4.2^{R28C}. (B) Quantitative analysis of Kir4.2^{WT} and Kir4.2^{R28C} protein levels using an unpaired t-test (**** P< 0.0001, N = 6). (C) A brief illustration of the N-linked glycosylation process and functions of enzymes PNGase F and Endo H. Created with BioRender.com (D) Western blot for assessing the glycosylation states of Kir4.2^{WT} and Kir4.2^{R28C} through treatment with PNGase F/EndoH. (E-F) Quantitative analysis of the overall glycosylation protein levels (E) and the ratio of mature (upper band) to immature (bottom band) proteins (F) following treatment with PNGAse/Endo H, analyzed by one-way ANOVA (** P < 0. 01, * P < 0. 05, N = 3-5).

Figure 4 Evaluation of the ER influence on the Kir4.2^{WT} and Kir4.2 ^{R28C} protein level difference. (A) Representative Western blot analysis showcasing the effects of tunicamycin on Kir4.2 protein synthesis. Kir4.2^{WT} and Kir4.2^{R28C} transfected HEK293T cells were treated with 1 µg/ml tunicamycin for 0 hours (negative control), 2 hours, or 6 hours prior to Western blot analysis. NT, Non-transfected; WT, Kir4.2^{WT}; MT, Kir4.2^{R28C}. (B-C) Quantitive analysis of the overall Kir4.2^{WT} and Kir4.2^{R28C} protein levels normalized to the WT 0 h condition (B) and the ratio of mature to immature proteins (C) with or without tunicamycin treatment, using one-way ANOVA (**** P < 0.0001, * P < 0. 05, N = 4). Binding Immunoglobulin Protein (BiP) served as a positive control for ER stress.

Figure 5 Investigation of the role of the ubiquitin-proteasome system (UPS) in Kir 4.2 channel regulation. (A) Schematic representation of cellular protein processing pathways and the mechanisms of action for MG132 and bafilomycin A1. Created with BioRender.com (B) Western blot analysis of Kir4.2^{WT} and Kir4.2^{R28C} in HEK293T cells transiently transfected and treated with 10 µM MG132 for 0 hours (negative control) and 8 hours. NT, Non-transfected; WT, Kir4.2^{WT}; MT, Kir4.2^{R28C}. (C-D) Quantitive evaluation of total Kir4.2^{WT} and Kir4.2^{R28C} protein levels (C) and the proportion of mature to immature protein forms (D) following MG132 treatment, assessed by unpaired t-test (* P < 0.05, N = 3).

Figure 6 Lysosomal degradation pathway influence on Kir4.2 channels regulation. (A) Western blot assessment of Kir4.2^{WT} and Kir4.2^{R28C} overexpressing HEK293T cells following treatment with 100 nM bafilomycin A1 (Baf A1) for 0 hours (negative control), 3 hours or 6 hours. NT, Non-transfected; WT, Kir4.2^{WT}; MT, Kir4.2^{R28C}. (B) Total protein expression levels of Kir4.2^{WT} and Kir4.2^{R28C} were analyzed, with results normalized to the WT 0 h condition for comparison. (C) Analysis of the ratio between mature and immature protein forms following Baf A1 treatment, evaluated by one-way ANOVA (* P < 0.05, N = 3). LC3B served as a positive control for lysosomal activity.

Figure 7 Differential plasma membrane trafficking of Kir4.2^{WT} and Kir4.2$^{p.\ R28C}$ assessed by immunofluorescence studies. (A-B) Representative immunofluorescence analysis of HEK293T cells transiently transfected with Kir4.2^{WT} (A) and Kir4.2^{R28C} (B) using specific antibodies for staining. Na^+/K^+-ATPase served as a marker for the plasma membrane. Images were acquired with an Olympus FV3000 confocal microscope at 60X magnification. (C-G) Quantitative analysis of Kir4.2 expression on the cell membrane involves (C) removal of redundant nuclear features through image processing techniques to enhance clarity, (D)

recognition and segmentation of nuclear regions within the cell, (E) calculation of cytoplasmic area surrounding the nuclei, (F) precise identification of the cell membrane region and subsequent calculation of Kir4.2 expression area utilizing advanced image analysis algorithms and (G) refinement of analysis to specifically identify and quantify the Kir4.2 expression area localized on the cell membrane. (H-I) Comparative plot profile analysis of membrane trafficking between $Kir4.2^{WT}$ and $Kir4.2^{R28C}$. The membrane expression of Kir4.2 channels was normalized to the plamsa membrane area defined by Na^+/K^+-ATPase signals (H) and total Kir4.2 expression throughout the cell (I), respectively. Statistical analysis was carried out using an unpaired t-test (*P< 0.05, **P< 0.01, $Kir4.2^{WT}$ N = 45, $Kir4.2^{R28C}$ N = 34).

Figure 1

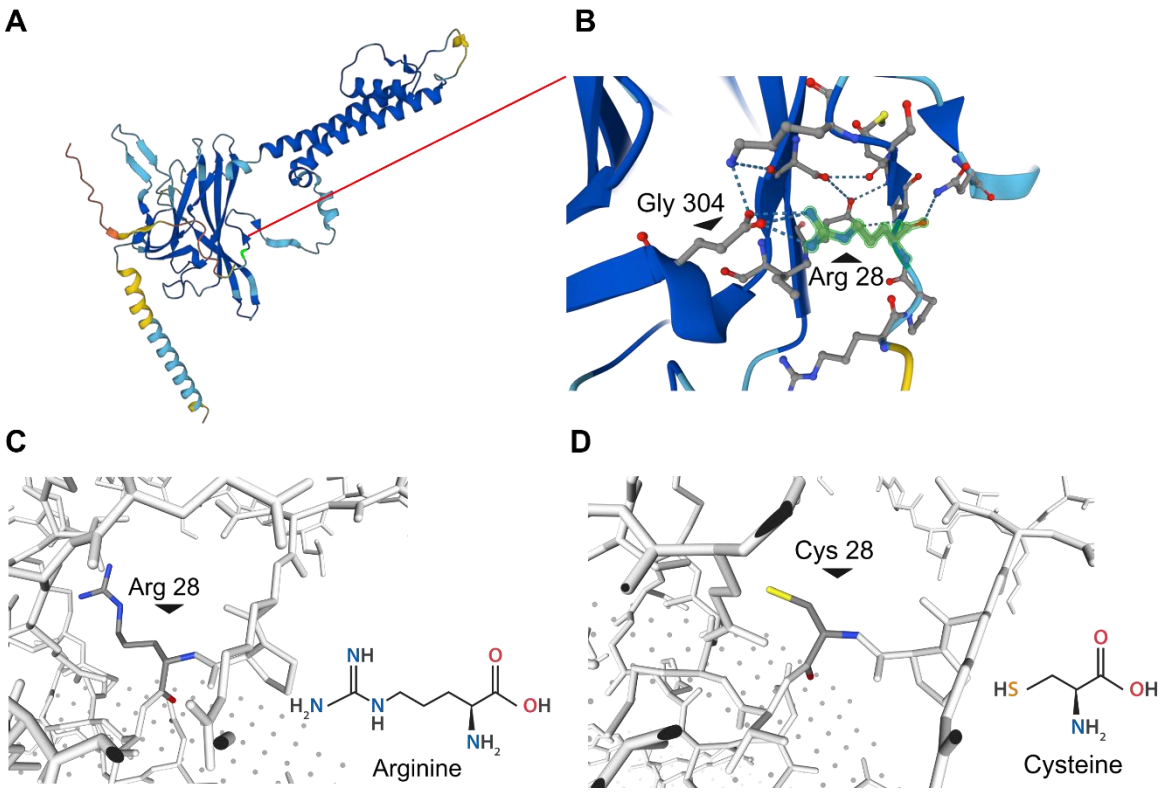
A
B
Gly 304
Arg 28
C
Arg 28
NH
O
H2N
N
H
OH
NH2
Arginine
D
Cys 28
O
HS
OH
NH2
Cysteine

Figure 2

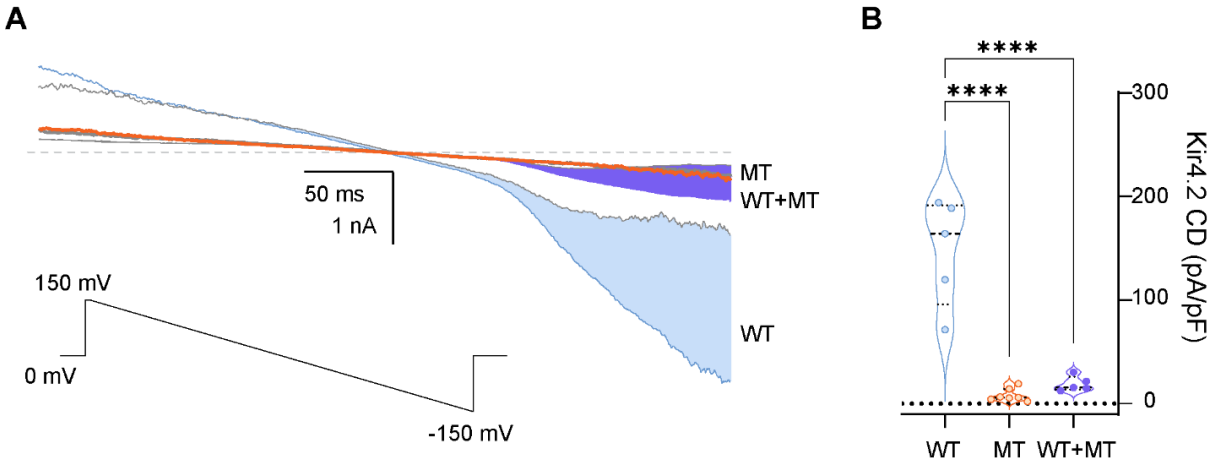
A
MT
WT+MT
WT
50 ms
1 nA
150 mV
0 mV
-150 mV
B
****
****
300
200
100
0
Kir4.2 CD (pA/pF)
WT
MT
WT+MT

Figure 3

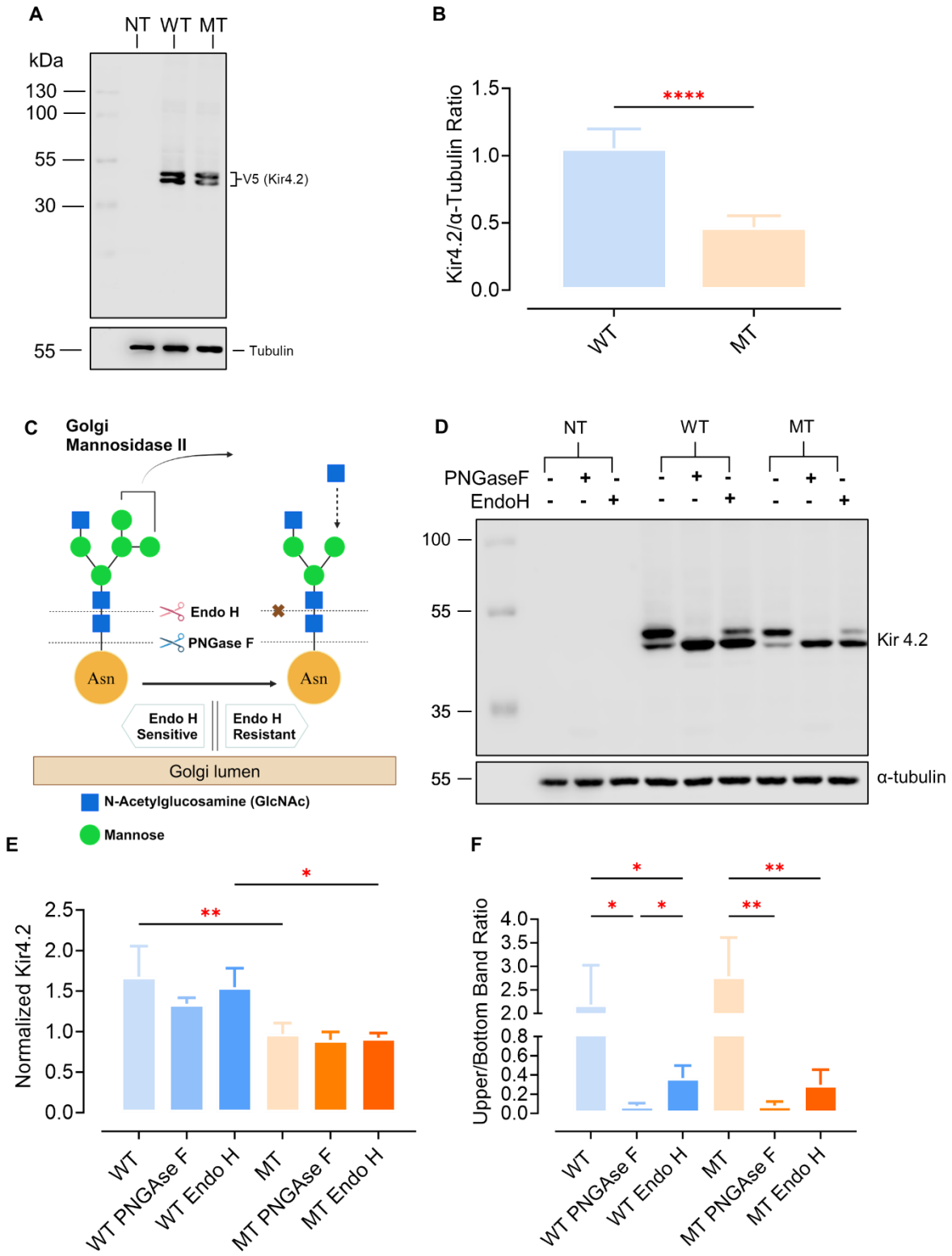
A
NT WT MT
kDa
130
100
55
30
V5 (Kir4.2)
55
Tubulin
B
Kir4.2/α-Tubulin Ratio
1.5
1.0
0.5
0.0
****
WT
MT
C
Golgi
Mannosidase II
Endo H
PNGase F
Asn
Asn
Endo H Sensitive
Endo H Resistant
Golgi lumen
N-Acetylglucosamine (GlcNAc)
Mannose
D
NT
WT
MT
PNGaseF
EndoH
100
55
35
55
Kir 4.2
α-tubulin
E
Normalized Kir4.2
2.5
2.0
1.5
1.0
0.5
0.0
**
*
WT
WT PNGAse F
WT Endo H
MT
MT PNGAse F
MT Endo H
F
Upper/Bottom Band Ratio
4.0
3.5
3.0
2.5
2.0
0.8
0.6
0.4
0.2
0.0
*
*
*
**
**
WT
WT PNGAse F
WT Endo H
MT
MT PNGAse F
MT Endo H

Figure 4

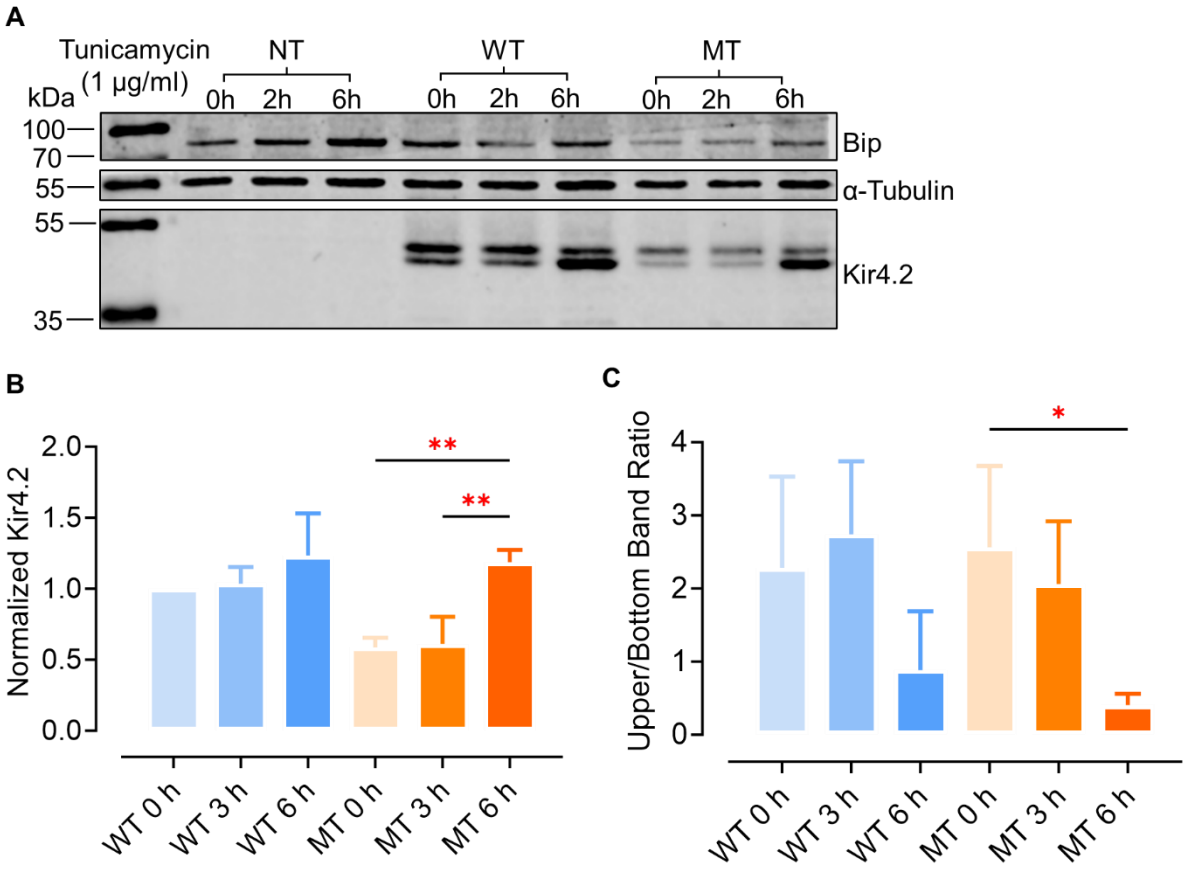
A
Tunicamycin
(1 μg/ml)
NT
WT
MT
kDa
0h
2h
6h
0h
2h
6h
0h
2h
6h
100
70
55
55
35
Bip
α-Tubulin
Kir4.2
B
Normalized Kir4.2
2.0
1.5
1.0
0.5
0.0
**
**
WT 0 h
WT 3 h
WT 6 h
MT 0 h
MT 3 h
MT 6 h
C
Upper/Bottom Band Ratio
4
3
2
1
0
*
WT 0 h
WT 3 h
WT 6 h
MT 0 h
MT 3 h
MT 6 h

Figure 5

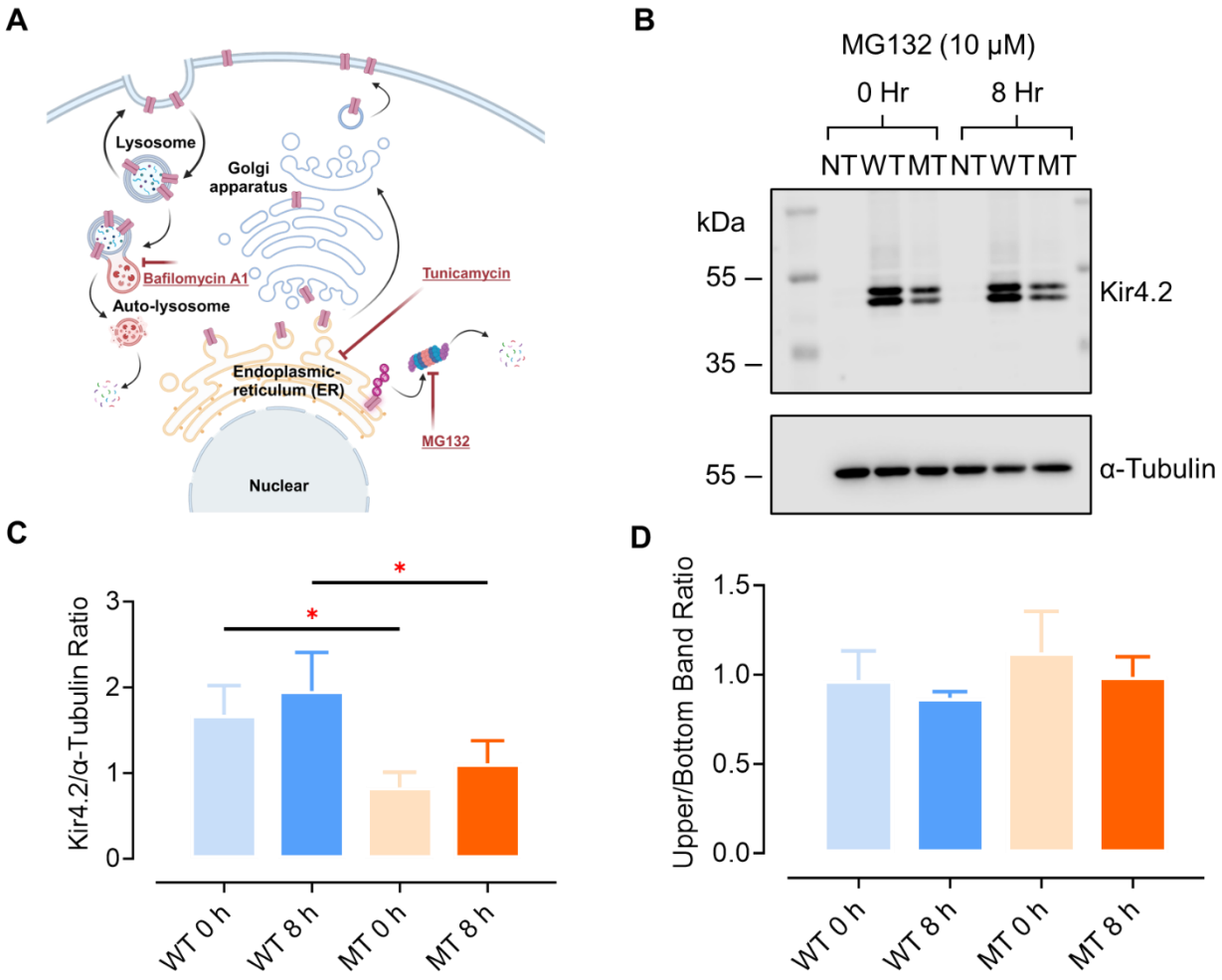
A
Lysosome
Golgi apparatus
Bafilomycin A1
Auto-lysosome
Tunicamycin
Endoplasmic-reticulum (ER)
MG132
Nuclear
B
MG132 (10 μM)
0 Hr
8 Hr
NTWTMTNTWTMT
kDa
55
35
Kir4.2
55
α-Tubulin
C
Kir4.2/α-Tubulin Ratio
3
2
1
0
*
*
WT 0 h
WT 8 h
MT 0 h
MT 8 h
D
Upper/Bottom Band Ratio
1.5
1.0
0.5
0.0
WT 0 h
WT 8 h
MT 0 h
MT 8 h

Figure 6

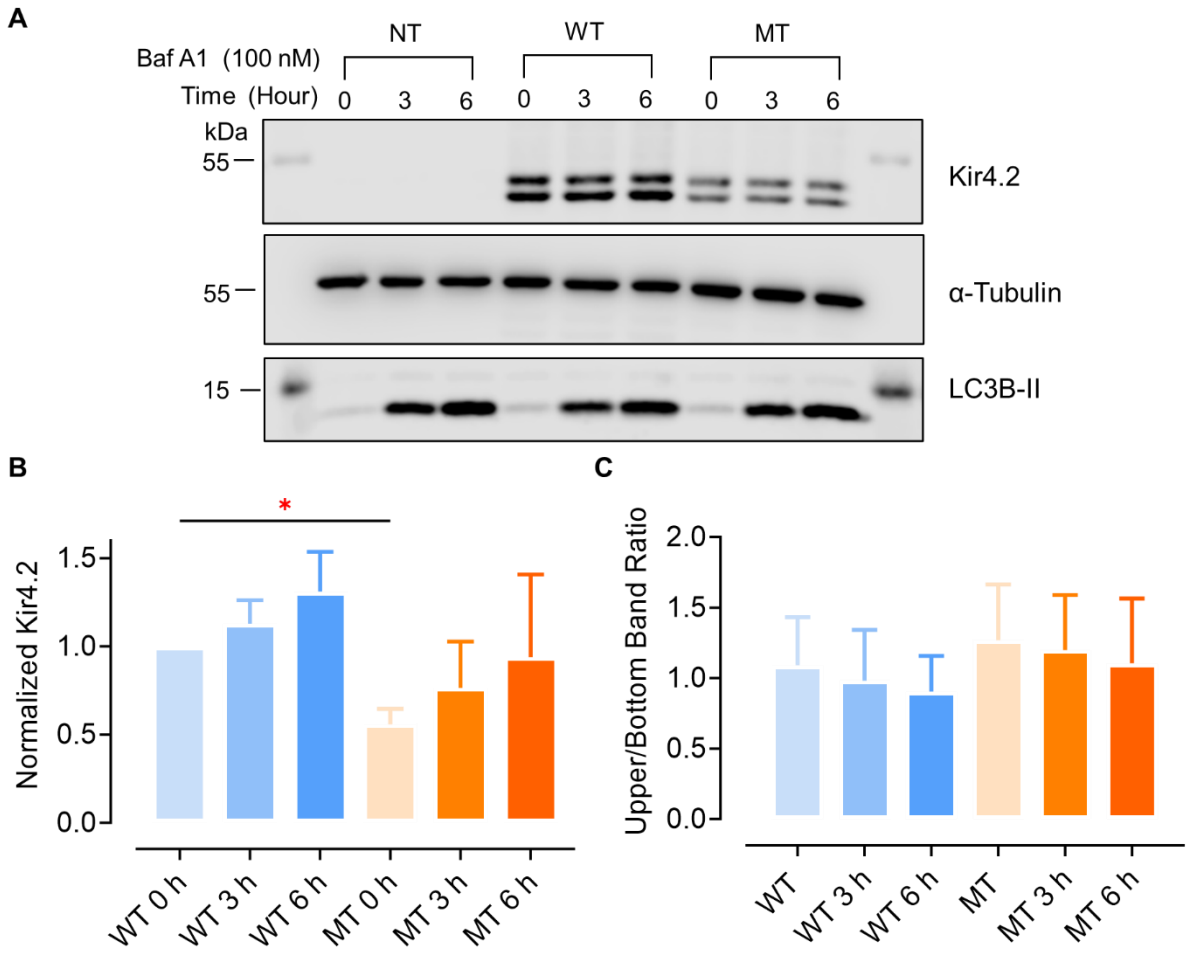
A
NT
WT
MT
Baf A1 (100 nM)
Time (Hour)
0 3 6 0 3 6 0 3 6
kDa
55
Kir4.2
55
α-Tubulin
15
LC3B-II
B
*
Normalized Kir4.2
1.5
1.0
0.5
0.0
WT 0 h
WT 3 h
WT 6 h
MT 0 h
MT 3 h
MT 6 h
C
Upper/Bottom Band Ratio
2.0
1.5
1.0
0.5
0.0
WT
WT 3 h
WT 6 h
MT
MT 3 h
MT 6 h

Figure 7

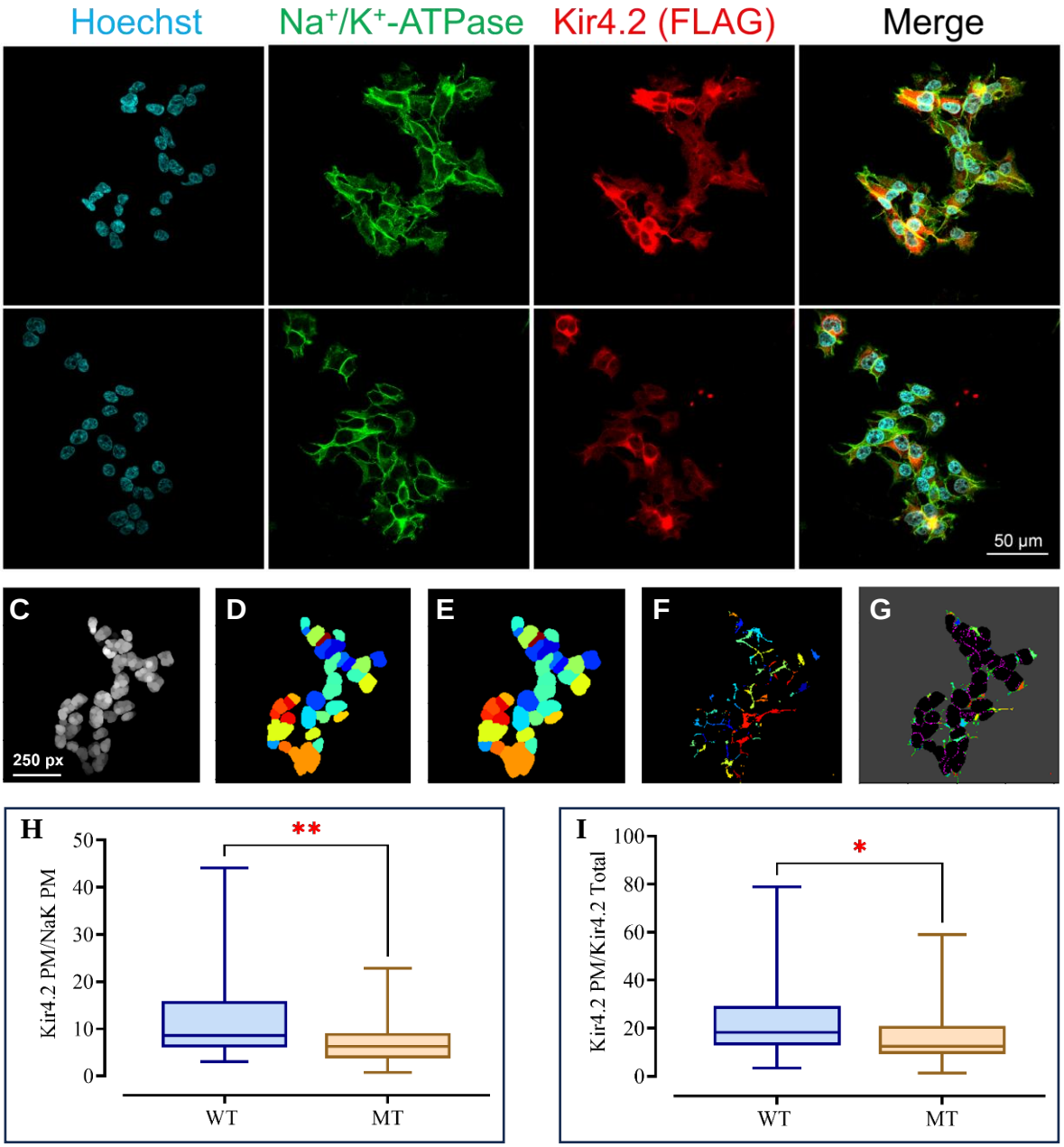
Hoechst
Na+/K+-ATPase
Kir4.2 (FLAG)
Merge
50 µm
C
D
E
F
G
250 px
H
Kir4.2 PM/NaK PM
50
40
30
20
10
0
**
WT
MT
I
Kir4.2 PM/Kir4.2 Total
100
80
60
40
20
0
*
WT
MT